Ankyrin repeat and zinc-finger domain-containing 1 mutations are associated with infantile-onset inflammatory bowel disease

Received for publication, December 12, 2016, and in revised form, March 13, 2017 Published, Papers in Press, March 16, 2017, DOI 10.1074/jbc.M116.772038

Désirée Y. van Haaften-Visser[‡§], Magdalena Harakalova[¶1], Enric Mocholi[§1,2], Joris M. van Montfrans[‡], Abdul Elkadri[‖], Ester Rieter[§], Karoline Fiedler[‖**], Peter M. van Hasselt[‡], Emily M. M. Triffaux[§3], Mieke M. van Haelst[¶], Isaac J. Nijman[¶], Wigard P. Kloosterman[¶], Edward E. S. Nieuwenhuis[‡], Aleixo M. Muise[‖**], Edwin Cuppen[‡‡], Roderick H. J. Houwen[‡], and Paul J. Coffer[‡§4]**

*From the [‡]Division of Pediatrics, Wilhelmina Children's Hospital, the [§]Regenerative Medicine Center and Center for Molecular Medicine, and the [¶]Department of Medical Genetics, Center for Molecular Medicine, University Medical Center Utrecht, 3584 CT Utrecht, The Netherlands, the [‖]Division of Gastroenterology, Hepatology, and Nutrition, Department of Pediatrics, University of Toronto, Hospital for Sick Children, Toronto, Ontario M5G 1X8, Canada, the **SickKids Inflammatory Bowel Disease Center and Cell Biology Program, Research Institute, Hospital for Sick Children, Toronto, Ontario M5G 1X8, Canada, and the [‡‡]Hubrecht Institute, KNAW and University Medical Center Utrecht, 3584 CT Utrecht, The Netherlands*

Edited by Dennis R. Voelker

Infantile-onset inflammatory bowel disease (IO IBD) is an invalidating illness with an onset before 2 years of age and has a complex pathophysiology in which genetic factors are important. Homozygosity mapping and whole-exome sequencing in an IO IBD patient and subsequent sequencing of the candidate gene in 12 additional IO IBD patients revealed two patients with two mutated ankyrin repeat and zinc-finger domain-containing 1 (*ANKZF1*) alleles (homozygous *ANKZF1* R585Q mutation and compound heterozygous *ANKZF1* E152K and V32_Q87del mutations, respectively) and two patients with one mutated *ANKZF1* allele. Although the function of ANKZF1 in mammals had not been previously evaluated, we show that ANKZF1 has an indispensable role in the mitochondrial response to cellular stress. ANKZF1 is located diffusely in the cytoplasm and translocates to the mitochondria upon cellular stress. ANKZF1 depletion reduces mitochondrial integrity and mitochondrial respiration under conditions of cellular stress. The *ANKZF1* mutations identified in IO IBD patients with two mutated *ANKZF1* alleles result in dysfunctional ANKZF1, as shown by an increased level of apoptosis in patients' lymphocytes, a decrease in mitochondrial respiration in patient fibroblasts with a homozygous *ANKZF1* R585Q mutation, and an inability of ANKZF1 R585Q and E152K to rescue the phenotype of yeast deficient in Vms1, the yeast homologue of ANKZF1. These data indicate that loss-of-function mutations in *ANKZF1* result in deregulation of mitochondrial integrity, and this may play a pathogenic role in the development of IO IBD.

Inflammatory bowel disease (IBD)[5] is a heterogeneous group of disorders, encompassing both Crohn's disease and ulcerative colitis, characterized by chronic inflammation of the gastrointestinal tract (1–3). The pathogenesis of IBD is complex and still largely unknown. It involves a disturbance of the intestinal mucosal homeostasis, which is an interplay of genetic factors, the intestinal microbiome, the immune system, and environmental factors (1–3). Genetic factors are especially important in infantile-onset IBD (IO IBD, defined as an onset before 2 years of age) (4), making this patient group particularly interesting for the purpose of investigating the genetic defects underlying IBD (5–7).

Next-generation sequencing (NGS) has been shown to be a valuable tool for increasing understanding of the genetic basis of human diseases and disease-causing pathways (8–10). For IO IBD patients, NGS has also led to the identification of several novel disease-causing mutations in genes including *IL10RA* (11), *IL10RB* (11), *IL10* (12), *XIAP* (13), *ADAM17* (14), and *TTC7A* (15). Using a combination of homozygosity mapping and whole-exome sequencing, we identified a homozygous mutation in the ankyrin repeat and zinc-finger domain-containing 1 (*ANKZF1*) gene in one IO IBD patient. We also defined compound heterozygous *ANKZF1* mutations in one additional IO IBD patient and a single heterozygous *ANKZF1* mutation in two additional IO IBD patients. Although the function of ANKZF1 in humans has not been previously described, valosin-containing protein (VCP)/cell division cycle 48 (Cdc48)-associated mitochondrial stress-responsive (Vms1), the yeast homologue of ANKZF1, has been demonstrated to be essential for mitochondrial protein degradation under stress conditions. Upon cellular stress, a complex containing Vms1 and Cdc48, a protein that has a role in endoplas-

The authors declare that they have no conflicts of interest with the contents of this article.

[1] Both authors contributed equally to this work.

[2] Supported by Dutch Rheumatology Foundation (ReumaFonds) Grant 2016-1-003.

[3] Supported by a Marie Curie Initial Training Network grant: European Translational tRaining for Autoimmunity and Immune manipulation Network (EU-TRAIN) Grant R2409.

[4] To whom correspondence should be addressed: Regenerative Medicine Center, University Medical Center Utrecht, Uppsalalaan 6, 3584 CT Utrecht, The Netherlands. Tel.: 31-88-755-7674; Fax: 31-88-755-5590; E-mail: p.j.coffer@umcutrecht.nl.

[5] The abbreviations used are: IBD, inflammatory bowel disease; IO IBD, infantile-onset inflammatory bowel disease; ECAR, extracellular acidification rate(s); EVS, Exome Variant Server; NGS, next-generation sequencing; NRA, non-reference allele; OCR, oxygen consumption rate(s); PBMC, peripheral blood mononuclear cell; PLA, proximity ligation assay; RPMI, Roswell Park Memorial Institute; SMD, synthetic minimal medium; VCP, valosin-containing protein; qRT-PCR, quantitative RT-PCR; ER, endoplasmic reticulum.

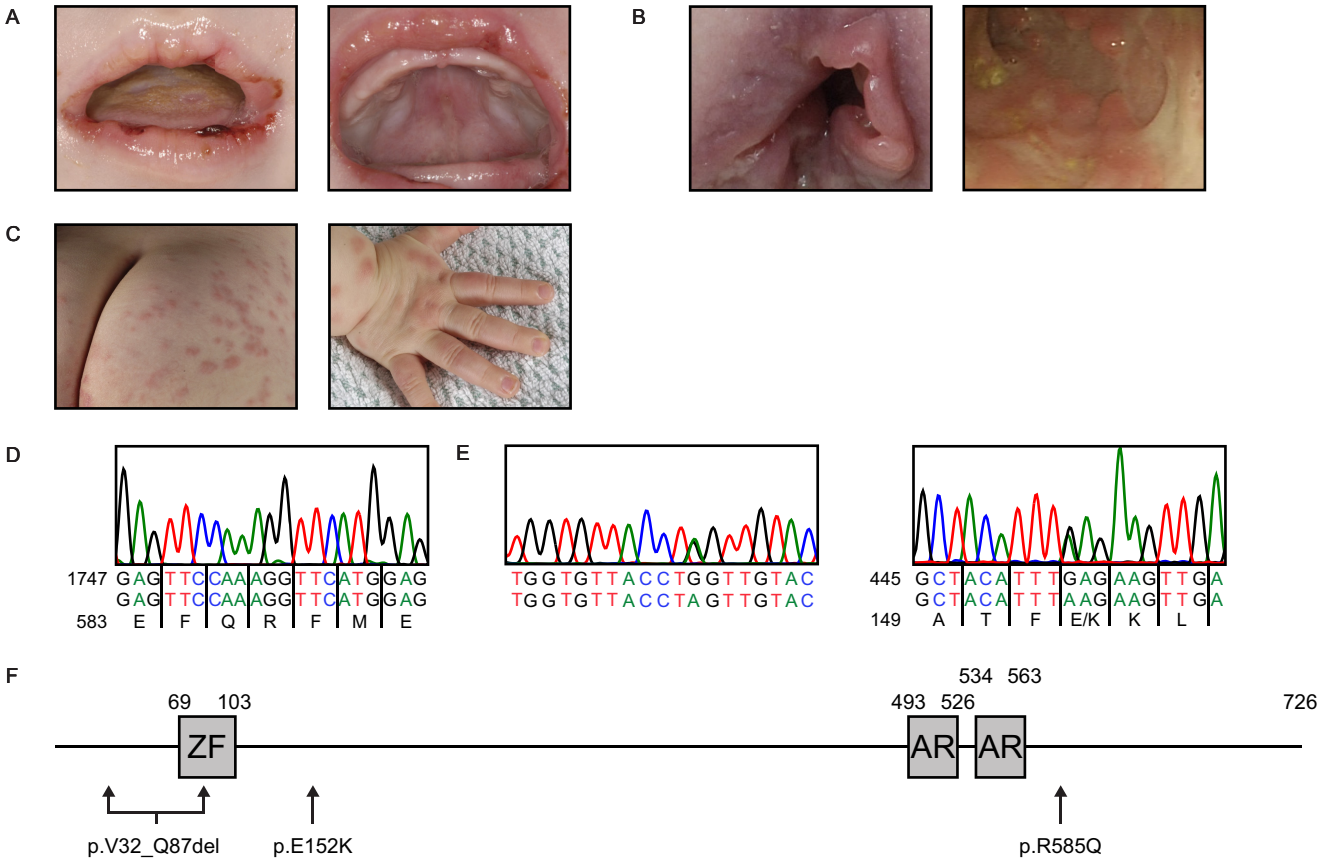

Figure 1. Two mutated ANKZF1 alleles in two patients with infantile-onset inflammatory bowel disease. *A*, perioral and oral inflammation of patient with homozygous *ANKZF1* R585Q mutation at 2 months of age. *B*, perianal and colonic inflammation of a patient with homozygous *ANKZF1* R585Q mutation at 2 months of age. *C*, skin anomalies of a patient with homozygous *ANKZF1* R585Q mutation at 10 months of age. *D*, Sanger sequencing of *ANKZF1* in peripheral blood-derived genomic DNA from a patient with homozygous *ANKZF1* R585Q mutation. *E*, Sanger sequencing of *ANKZF1* in peripheral blood-derived genomic DNA from a patient with compound heterozygous *ANKZF1* V32_Q87del and E152K mutations. *F*, schematic diagram of ANKZF1 protein structure, including one zinc finger (*ZF*) and two ankyrin repeats (*AR*). *ANKZF1* mutations identified in patients with two mutated *ANKZF1* alleles are indicated.

mic reticulum-associated protein degradation, translocates from the cytoplasm to the mitochondria, where it regulates the degradation of damaged, misfolded, and ubiquitinated proteins. Vms1 deficiency results in decreased ubiquitin-dependent mitochondrial protein degradation, leading to accumulation of damaged and misfolded mitochondrial proteins, causing mitochondrial dysfunction and subsequently apoptosis (16).

Here we show for the first time that mammalian ANKZF1 has a role in the mitochondrial response to cellular stress. ANKZF1 depletion reduces mitochondrial integrity and mitochondrial respiration under conditions of cellular stress, and mutations identified in the IO IBD patients with two mutated *ANKZF1* alleles also result in loss of ANKZF1 function. Although mitochondrial pathology has been observed previously in IBD patients, this is the first time that underlying mutations have been identified that provide evidence for a link between mitochondrial stress and the pathogenesis of IBD. These findings provide a novel molecular mechanism in the pathophysiology of IO IBD.

Results

Mutation of ANKZF1 in four patients with infantile-onset inflammatory bowel disease

The female index patient presented at the age of 6 weeks with loose stools containing blood and mucus as well as severe ulcerative skin lesions at the perioral and perianal regions and extremities (Fig. 1, *A* and *B*). At endoscopy, extensive ulcerating lesions were found in the mouth and the entire colon, including the rectosigmoid (Fig. 1*B*). Histology of colonic biopsies showed extensive lymphocytic infiltration of the lamina propria without distortion of crypt architecture. A biopsy of a skin lesion showed an epidermis distorted by lymphocytic and granulocytic infiltrate. Immunological investigations of peripheral blood showed severe lymphopenia in T cells, B cells, and NK cells with typical total lymphocyte counts $< 0.5{\cdot}10^9$/liter but with normal percentages of naive $CD4^+$ and $CD8^+$ T cells. Based on the clinical signs and histological abnormalities in combination with the exclusion of an infectious or allergic cause, the diagnosis IO IBD was made. Although the clinical phenotype resembled the phenotype of patients with IL10 deficiency, no mutations were found in *IL10*, *IL10RA*, and *IL10RB*, as well as in several other genes known to be associated with IBD (including *RAG1*, *RAG2*, *DOCK8*, and chronic granulomatous disease (CGD)-related genes). Immunosuppressive treatment with corticosteroids was started with a marked response on both ulcerating skin lesions and colitis. After complete resolution of symptoms, azathioprine was started (2 mg/kg/day), and corticosteroids were tapered; however, skin lesions recurred, although with a milder (non-ulcerating) phenotype (Fig. 1*C*). During follow-up until the age of 5 years, low-

grade ulcerative skin lesions as well as signs of residual gut inflammation persisted, with frequent periods of non-infectious diarrhea containing mucus and continuous elevations of fecal calprotectin levels. Concurrent with the lymphopenia, hypogammaglobulinemia was noted, and prophylactic antibiotics were prescribed. No severe or opportunistic infections were noted.

Because the parents are second cousins, an autosomal recessive inherited cause of the IBD was suspected. Homozygosity mapping resulted in six regions larger than 2 Mb. With whole-exome sequencing, only one novel homozygous mutation was identified that was not present in our in-house database: g.220100258G>A (c.1754G>A, p.R585Q, NM_018089.2) in *ANKZF1*. This mutation, as well as its segregation, was confirmed by Sanger sequencing (Fig. 1, *D* and *F*). Twelve additional patients with IO IBD, of which three had a disease onset before 6 months of age, were screened for mutations in *ANKZF1*. In all three patients in which symptoms initiated before 6 months of age, *ANKZF1* mutations were identified, whereas no *ANKZF1* mutations were found in the patients with a disease onset between 6 and 24 months of age. One boy carried compound heterozygous *ANKZF1* mutations: g.220096885G>A, resulting in skipping of half of exon 2 and exon 3 (p.V32_Q87del), and g.220097301G>A (c.454G>A, p.E152K) (Fig. 1, *E* and *F*). This patient presented in the first 6 months of life with a pancolitis. In this boy, no skin inflammation or lymphopenia was present. Two other patients were found to have a single heterozygous *ANKZF1* mutation: g.220094405C>T, located in the promotor of *ANKZF1*, and g.220100539A>C (c.1913A>C, p.Q638P), respectively. Taken together, two IO IBD patients carried a mutation on both *ANKZF1* alleles, and two additional patients were found to have a single mutated *ANKZF1* allele.

ANKZF1 mRNA and protein expression are reduced in an IO IBD patient with homozygous ANKZF1 R585Q mutation

First, it was determined whether *ANKZF1* mutations may influence ANKZF1 mRNA and protein expression. In fibroblasts and peripheral blood mononuclear cells (PBMCs) from the patient with a homozygous *ANKZF1* R585Q mutation, *ANKZF1* mRNA expression levels were clearly reduced (Fig. 2, *A* and *B*), whereas in EBV-transformed B-lymphocytes, reduced expression was also evident (Fig. 2*C*). All three cell types also exhibited reduced ANKZF1 protein expression (Fig. 2, *A*–*C*). In EBV-transformed B-lymphocytes from the patient with the compound heterozygous *ANKZF1* V32_Q87del and E152K mutations, ANKZF1 mRNA and protein expression were equal to the ANKZF1 levels in control cells (Fig. 2*D*).

To test whether the decline in protein expression in the patient with a homozygous *ANKZF1* R585Q mutation may also be due to an increased proteasomal degradation of ANKZF1, fibroblasts and EBV-transformed B-lymphocytes were left untreated or treated with the proteasome inhibitor MG132, and ANKZF1 protein levels were analyzed. Treatment with MG132 did not affect ANKZF1 protein expression levels (Fig. 2, *E* and *F*). Subsequently, U2OS cells transfected with FLAG-ANKZF1 wild type (WT), FLAG-ANKZF1 R585Q, or FLAG-ANKZF1 E152K were incubated with or without MG132, and ANKZF1 protein levels were evaluated. Cells transfected with FLAG-FOXP3 were used as a positive control, because we have previously shown FOXP3 levels to increase upon MG132 treatment (17). Again, no change in ANKZF1 protein level was detected (Fig. 2*G*). These data suggest that the reduced ANKZF1 protein expression is not due to increased proteasomal degradation. To further confirm that the stability of ANKZF1 is not influenced by R585Q or E152K mutations, cells transfected with FLAG-ANKZF1 WT, FLAG-ANKZF1 R585Q, or FLAG-ANKZF1 E152K were incubated with or without cycloheximide, an inhibitor of protein translation, and ANKZF1 protein levels were determined. Again cells transfected with FLAG-FOXP3 were used as positive control, because treatment with cycloheximide decreases FOXP3 levels (17). In cells transfected with WT or with mutated ANKZF1, no change in ANKZF1 protein expression was observed between the untreated and treated cells, indicating a similar turnover of WT and mutated ANKZF1 (Fig. 2*H*).

Taken together, these data show that the *ANKZF1* R585Q mutation causes reduced ANKZF1 mRNA and protein expression, whereas ANKZF1 protein stability is unaffected. However, *ANKZF1* mutations do not *per se* affect ANKZF1 mRNA and protein expression, as illustrated by the IO IBD patient with compound heterozygous *ANKZF1* V32_87del and E152K mutations.

ANKZF1 R585Q mutation exhibits reduced stress-induced mitochondrial translocation

A recent study has shown that the yeast ANKZF1 homologue, Vms1, constitutively interacts with Cdc48, the yeast orthologue of human VCP. Under conditions of cellular stress, this complex translocates to mitochondria, where it regulates the degradation of damaged, misfolded, and ubiquitinated proteins (16). To investigate whether cellular stress may also regulate mitochondrial translocation of ANKZF1 and whether this may be influenced by R585Q and E152K mutations, U2OS cells were first left untreated or exposed to hydrogen peroxide (H_2O_2). ANKZF1 localization was determined by confocal microscopy. In untreated cells, ANKZF1 was localized diffusely in the cytoplasm. However, upon exposure to H_2O_2, a translocation toward the mitochondria was observed (Fig. 3*A*). To evaluate the consequences of the *ANKZF1* R585Q and E152K mutation, cells co-transfected with HA-VCP and FLAG-ANKZF1 WT, FLAG-ANKZF1 R585Q, or FLAG-ANKZF1 E152K were untreated or exposed to H_2O_2. Localization of ANKZF1 and VCP was visualized by confocal microscopy. In untreated cells, VCP and both WT and mutant ANKZF1 were located diffusely in the cytoplasm. Exposure of the cells to H_2O_2 resulted in translocation of ANKZF1 and VCP toward the mitochondria. This translocation was reduced in cells transfected with ANKZF1 R585Q, but not in cells transfected with ANKZF1 E152K (Fig. 3*B*).

To determine whether this reduced translocation of ANKZF1 R585Q upon exposure to H_2O_2 is the result of a disrupted interaction between ANKZF1 R585Q and VCP, cells co-transfected with HA-VCP and FLAG-ANKZF1 WT, FLAG-ANKZF1 R585Q, or FLAG-ANKZF1 E152K were left untreated or exposed to H_2O_2. FLAG-ANKZF1 was immunoprecipitated, after which the VCP and ANKZF1 protein association was visualized by Western blotting. In cells that were not exposed to

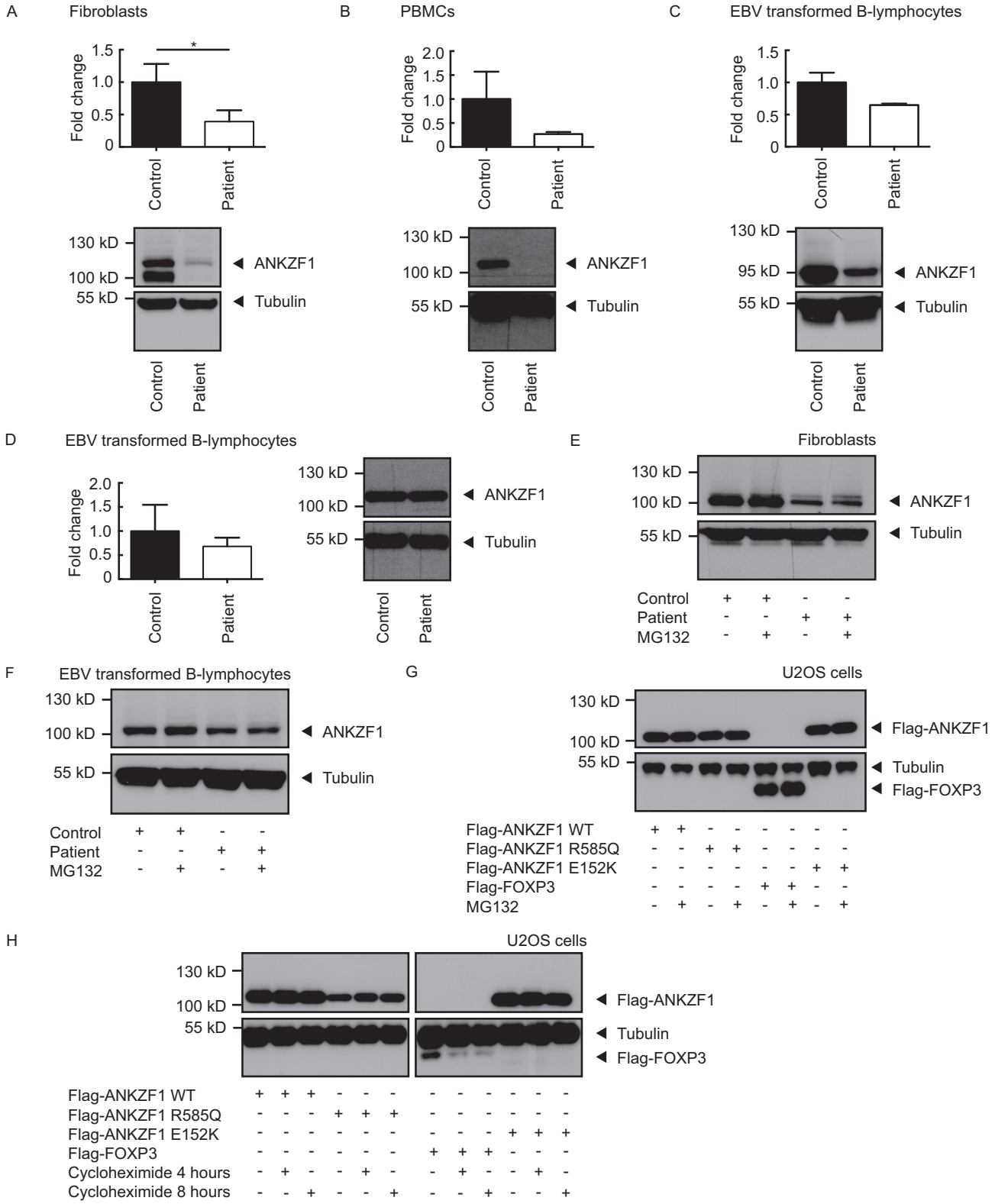

Figure 2. ANKZF1 mRNA and protein expression are reduced in an IO IBD patient with homozygous ANKZF1 R585Q mutation. *A–C*, qRT-PCR and Western-blotting analysis of ANKZF1 mRNA and protein expression, respectively, in fibroblasts (*A*), PBMCs (*B*), and EBV-transformed B-lymphocytes (*C*) of a healthy control and patient with homozygous *ANKZF1* R585Q mutation. *D*, qRT-PCR and Western-blotting analysis of ANKZF1 mRNA and protein expression, respectively, in EBV-transformed B-lymphocytes of a healthy control and patient with compound heterozygous *ANKZF1* V32_Q87del and E152K mutations. *E* and *F*, fibroblasts (*E*) and EBV-transformed B-lymphocytes (*F*) of a healthy control and patient with homozygous *ANKZF1* R585Q mutation were left untreated or treated with 2 μM MG132 for 16 h. Protein expression was determined by Western-blotting analysis using anti-ANKZF1 and anti-tubulin antibodies. *G* and *H*, U2OS cells were transfected with the indicated constructs. Cells were left untreated, treated with 2 μM MG132 for 16 h (*G*), or treated with 5 μg/ml cycloheximide for 4 or 8 h (*H*). Protein expression was determined by Western-blotting analysis using anti-FLAG and anti-tubulin antibodies. For qRT-PCR analyses, average and S.D. (*error bars*) of three independent experiments are shown. For Western-blotting analyses, results are representative of three independent experiments. *, $p \leq 0.05$.

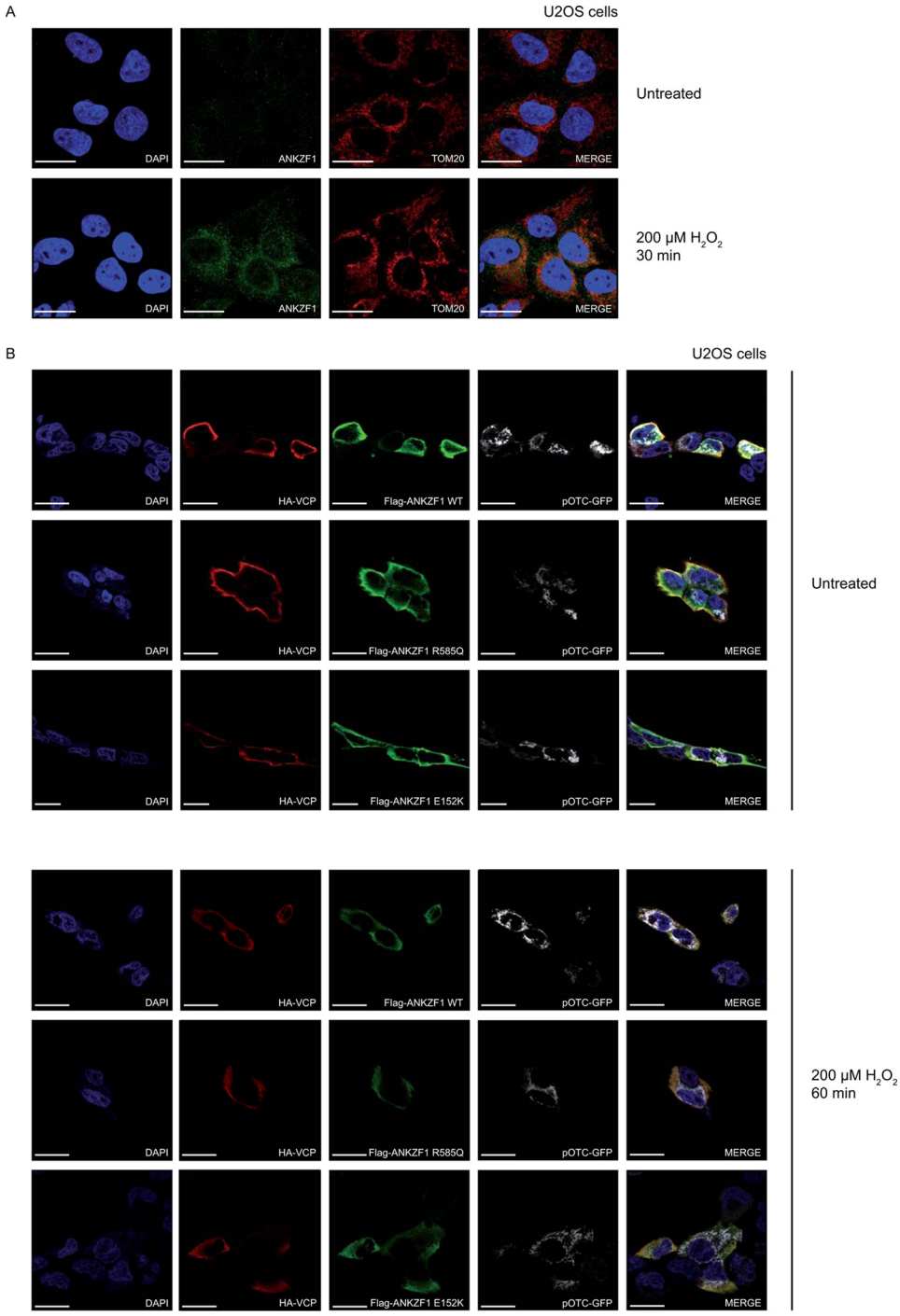

Figure 3. ANKZF1 R585Q mutation exhibits reduced stress-induced mitochondrial translocation. *A*, U2OS cells were left untreated or treated with 200 μM H_2O_2 for 30 min. ANKZF1 and TOM20 were visualized by immunofluorescence microscopy using anti-ANKZF1 and anti-TOM20 antibodies. TOM20 was used as a mitochondrial marker. DAPI was used to visualize the nuclei. *Scale bars*, 25 μm. *B*, U2OS cells were co-transfected with the indicated constructs and left untreated or treated with 200 μM H_2O_2 for 60 min. HA-VCP and FLAG-ANKZF1 were visualized by immunofluorescence microscopy using anti-HA and anti-FLAG antibodies. pOTC-GFP was used as a mitochondrial marker. DAPI was used to visualize the nuclei. *Scale bars*, 25 μm. *C*, U2OS cells were co-transfected with the indicated constructs and left untreated or treated with 200 or 500 μM H_2O_2 for 90 min. A co-immunoprecipitation (*Co-IP*) was performed using anti-FLAG beads. ANKZF1-VCP interaction was determined by Western-blotting analysis using anti-FLAG and anti-HA antibodies. *D*, U2OS cells were co-transfected with the indicated constructs and exposed to 0 or 200 μM H_2O_2 for 60 min. A PLA was performed. Punctate staining (*red*) indicates a VCP-ANKZF1 interaction. DAPI was used to visualize the nuclei. *Scale bars*, 25 μm. Results are representative of three independent experiments.

H_2O_2, ANKZF1 was already associated with VCP, indicating that interaction was independent of levels of cellular stress. Association of ANKZF1 and VCP was unaffected in ANKZF1 R585Q and E152K mutants. Furthermore, in cells transfected with either WT or mutated ANKZF1, exposure to H_2O_2 did not influence association between VCP and ANKZF1 (Fig. 3*C*). To further validate these results, cells co-transfected with HA-VCP and FLAG-ANKZF1 WT, FLAG-ANKZF1 R585Q, or FLAG-ANKZF1 E152K were untreated or exposed to H_2O_2, and an *in situ* proximity ligation assay (PLA) was per-

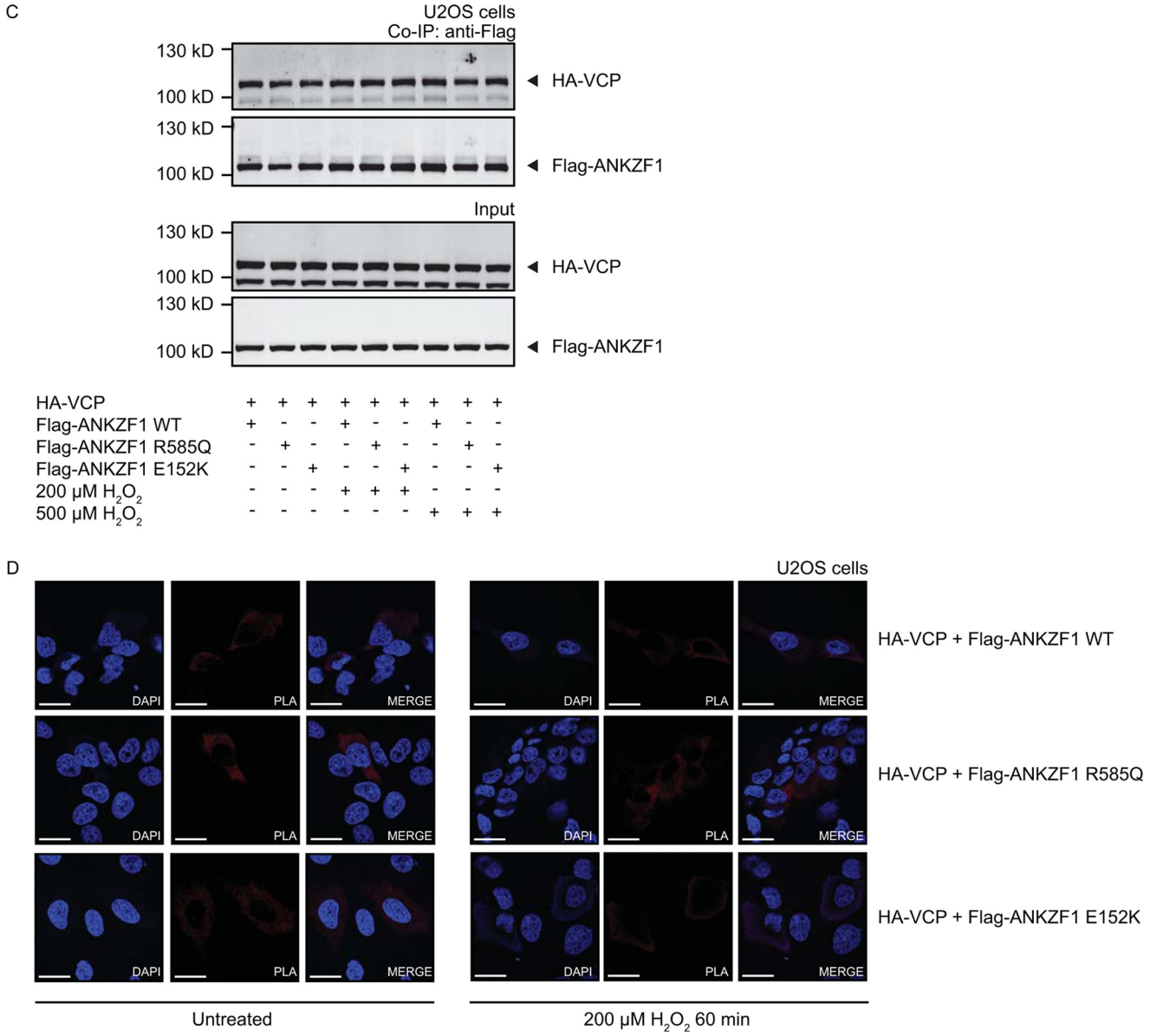

Figure 3—*continued*

formed. This technique allows visualization of protein-protein interactions, because a PLA signal is only obtained when proteins are in very close proximity to each other. Interaction was observed between FLAG-ANKZF1 WT and VCP in both treated and untreated cells, and this interaction was similar for ANKZF1 R585Q and E152K mutants (Fig. 3*D*).

Taken together, these data show that, similar to the yeast Cdc48-Vms1 complex, the VCP-ANKZF1 complex translocates toward the mitochondria under conditions of cellular stress. This translocation is reduced in the ANKZF1 R585Q mutant, whereas interaction between VCP and ANKZF1 is unaffected.

ANKZF1 depletion reduces mitochondrial integrity and mitochondrial respiration under conditions of cellular stress

In yeast, deficiency of the ANKZF1 homologue Vms1 causes accumulation of damaged mitochondrial proteins and subsequently mitochondrial dysfunction (16). To determine the effect of deficiency of ANKZF1 on mitochondrial integrity and mitochondrial function, an ANKZF1-knockdown cell line was generated, resulting in a reduction of ANKZF1 protein expression by ~60%. A control line was also generated by transduction of U2OS cells with a lentiviral construct containing scrambled shRNA (Fig. 4*A*). To investigate mitochondrial integrity, cells with and without ANKZF1 knockdown were left untreated or exposed to H_2O_2, after which they were stained with rhodamine-123 and analyzed by FACS. Rhodamine-123 selectively accumulates in mitochondria in a mitochondrial-membrane potential-dependent manner. Under basal conditions, mitochondrial integrity was similar between cells with or without ANKZF1 knockdown. However, induction of cellular stress by H_2O_2 treatment caused a time-dependent decrease in mitochondrial integrity when ANKZF1 levels were reduced (Fig. 4, *B* and *C*).

To investigate the effect of ANKZF1 depletion on mitochondrial function, cells were left untreated or exposed to H_2O_2, and oxygen consumption rates (OCR) and extracellular acidification rates (ECAR) were determined using Seahorse metabolic

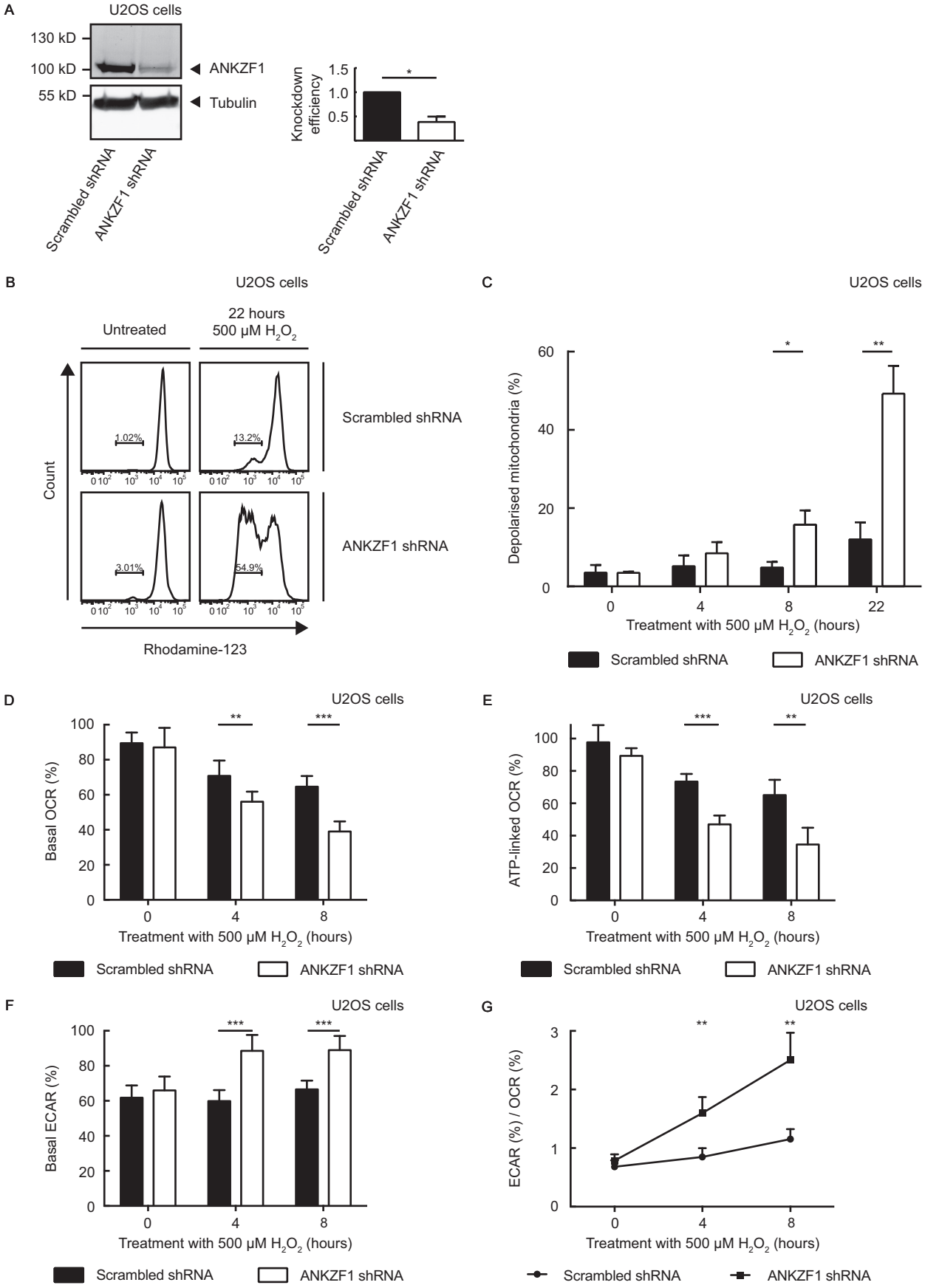
A
U2OS cells
130 kD
100 kD
55 kD
ANKZF1
Tubulin
Scrambled shRNA
ANKZF1 shRNA
Knockdown efficiency
1.5
1.0
0.5
*
B
U2OS cells
Untreated
22 hours
500 μM H2O2
Scrambled shRNA
ANKZF1 shRNA
Count
1.02%
13.2%
3.01%
54.9%
Rhodamine-123
C
U2OS cells
Depolarised mitochondria (%)
Treatment with 500 μM H2O2 (hours)
Scrambled shRNA
ANKZF1 shRNA
D
U2OS cells
Basal OCR (%)
Treatment with 500 μM H2O2 (hours)
E
U2OS cells
ATP-linked OCR (%)
F
U2OS cells
Basal ECAR (%)
G
U2OS cells
ECAR (%) / OCR (%)

flux analyzer technology, both at baseline and after treatment of the cells with drugs affecting mitochondrial respiration. In untreated cells, the basal mitochondrial respiration was similar between ANKZF1-knockdown and control cells. However, the observed reduction in basal OCR after induction of cellular stress was more pronounced in ANKZF1-knockdown cells than in control cells (Fig. 4*D*). This leads to a decreased ATP production in ANKZF1-knockdown cells under stress conditions, as shown by a more pronounced reduction in ATP-linked mitochondrial respiration in these cells compared with control cells (Fig. 4*E*), as evaluated after oligomycin treatment to block the mitochondrial H^+-ATP synthase. To investigate whether the decrease in mitochondrial respiration in ANKZF1-knockdown cells also influences glycolysis, ECAR was determined, which was increased in ANKZF1-knockdown cells exposed to H_2O_2 (Fig. 4*F*). This indicates that in ANKZF1-knockdown cells treated with H_2O_2, glycolytic activity is increased, most likely to compensate for the decrease in mitochondrial respiration (Fig. 4*G*). These data demonstrate that ANKZF1 deficiency results in both a loss of mitochondrial integrity and a decrease in mitochondrial respiration under conditions of cellular stress.

Increased apoptosis in lymphocytes harboring ANKZF1 mutations

It is known that mitochondrial dysfunction can ultimately lead to apoptosis (18, 19). To investigate whether the *ANKZF1* mutations identified in patients with two mutated *ANKZF1* alleles cause dysfunction of ANKZF1, the effect of the mutations on apoptosis was studied. First, to determine whether cell expansion is influenced by the *ANKZF1* mutations, EBV-transformed B-lymphocytes from both IO IBD patients with two mutated *ANKZF1* alleles and a healthy control were cultured, and cell numbers were determined daily. Decreased proliferative capacity of EBV-transformed B-lymphocytes from both patients was observed (Fig. 5*A*).

To investigate whether decreased cell numbers were due to increased apoptosis, patient-derived EBV-transformed B-lymphocytes were left untreated or treated with H_2O_2, and numbers of apoptotic cells were determined. EBV-transformed B-lymphocytes from both patients exposed to H_2O_2 exhibited a higher level of apoptosis compared with control EBV-transformed cell lines. Interestingly, in untreated EBV-transformed B-lymphocytes, the initial level of apoptosis was also higher in the patients' cells, which suggests increased basal levels of cellular stress (Fig. 5, *B* and *C*).

Subsequently, it was investigated whether the *ANKZF1* R585Q mutation also causes increased levels of apoptosis in patient lymphocytes. PBMCs were left untreated or treated with H_2O_2, and numbers of apoptotic T- and B-lymphocytes were determined. Apoptosis was significantly higher in both T-lymphocytes and B-lymphocytes from the IO IBD patient compared with healthy controls, either when the cells were left untreated or when they were exposed to H_2O_2 (Fig. 5, *D*–*G*).

To investigate whether this increased level of apoptosis could be the result of decreased mitochondrial respiration, fibroblasts from the patient with a homozygous *ANKZF1* R585Q mutation were left untreated or treated with H_2O_2, and OCR and ECAR were determined. In untreated cells, the basal OCR was significantly decreased in patient fibroblasts compared with control fibroblasts (Fig. 5*H*), resulting in decreased ATP production (Fig. 5*I*), a trend that was also present after treatment with H_2O_2 (Fig. 5, *H* and *I*). ECAR was increased in untreated patient fibroblasts (Fig. 5*J*). These data suggest that the *ANKZF1* R585Q mutation results in an increased glycolytic activity (Fig. 5*K*) to compensate for the decrease in mitochondrial respiration, even in cells not treated with H_2O_2.

To determine whether decreased mitochondrial respiration could be coupled with changes in autophagic flux, fibroblasts from the patient with a homozygous *ANKZF1* R585Q mutation were left untreated or treated with hydroxychloroquine, and protein expression of autophagy markers LC3-II and p62 was determined by Western blotting. However, no differences in autophagic flux were observed between patient and control cells (data not shown).

Taken together, these data demonstrate that *ANKZF1* mutations found in the patients with two mutated *ANKZF1* alleles may result in increased lymphocyte apoptosis, and the *ANKZF1* R585Q mutation causes a decrease in mitochondrial respiration but does not affect autophagy.

ANKZF1 R585Q and E152K are unable to functionally rescue Vms1-deficient yeast

Our data suggest that human ANKZF1 has a function similar to that of Vms1 in yeast. *ANKZF1* mutations found in the IO IBD patients with two mutated *ANKZF1* alleles led to an increased level of apoptosis, suggesting that these mutations result in loss of ANKZF1 function. To confirm this, the ability of WT and mutant ANKZF1 to rescue the loss of Vms1 in yeast was studied. A BY4742 **Δ***Vms1* yeast strain was transformed with a pRS416 vector containing GFP-tagged Vms1, ANKZF1 WT, ANKZF1 R585Q, or ANKZF1 E152K. Expression of all ANKZF1 constructs was equal, although levels were reduced compared with Vms1 (Fig. 6*A*). These yeast strains, together with a BY4742 WT and a BY4742 **Δ***Vms1* yeast strain transformed with pRS416 empty vector, were grown on synthetic minimal medium (SMD) plates without uracil with or without 3 mM H_2O_2. Under normal growth conditions, no difference in growth of the different yeast strains was observed (Fig. 6*B*). However, treatment with 3 mM H_2O_2 resulted in a reduction of BY4742 **Δ***Vms1* yeast growth compared with BY4742 WT yeast

Figure 4. ANKZF1 depletion reduces mitochondrial integrity and mitochondrial respiration under conditions of cellular stress. *A*, U2OS ANKZF1-knockdown and control cell lines were generated. Knockdown efficiency of ANKZF1 was determined by Western-blotting analysis and quantified relative to the control cell line. Differences in loading were compensated. Average and S.D. (*error bars*) of three independent experiments are shown. *B*, U2OS ANKZF1-knockdown and control cell line were left untreated or exposed to 500 μM H_2O_2 for 4, 8, or 22 h. The percentage of cells with depolarized mitochondria was determined by FACS using rhodamine-123. Graphs of untreated U2OS cells and U2OS cells treated for 22 h are shown. Results are representative of three independent experiments. *C*, percentage of U2OS ANKZF1-knockdown and control cells with depolarized mitochondria as determined by FACS after treatment with 500 μM H_2O_2 as indicated and staining with rhodamine-123. Average and S.D. of three independent experiments are shown. *D*–*G*, U2OS ANKZF1-knockdown and control cell line were left untreated or exposed to 500 μM H_2O_2 for 4 or 8 h. Basal OCR (*D*), ATP-linked OCR (*E*), ECAR (*F*), and ratio of basal ECAR and basal OCR (*G*) were determined using the XF-24 extracellular flux analyzer. OCR and ECAR are shown as percentages of the highest rate. Average and S.D. of two independent experiments are shown. *, $p \leq 0.05$; **, $p \leq 0.01$; ***, $p \leq 0.001$.

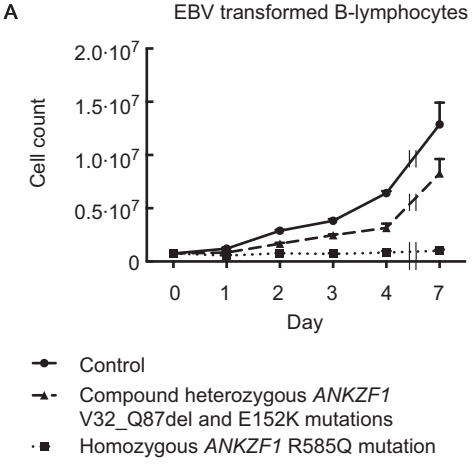
A
EBV transformed B-lymphocytes
Cell count
2.0·10^7
1.5·10^7
1.0·10^7
0.5·10^7
0
0 1 2 3 4 7
Day
Control
Compound heterozygous ANKZF1 V32_Q87del and E152K mutations
Homozygous ANKZF1 R585Q mutation

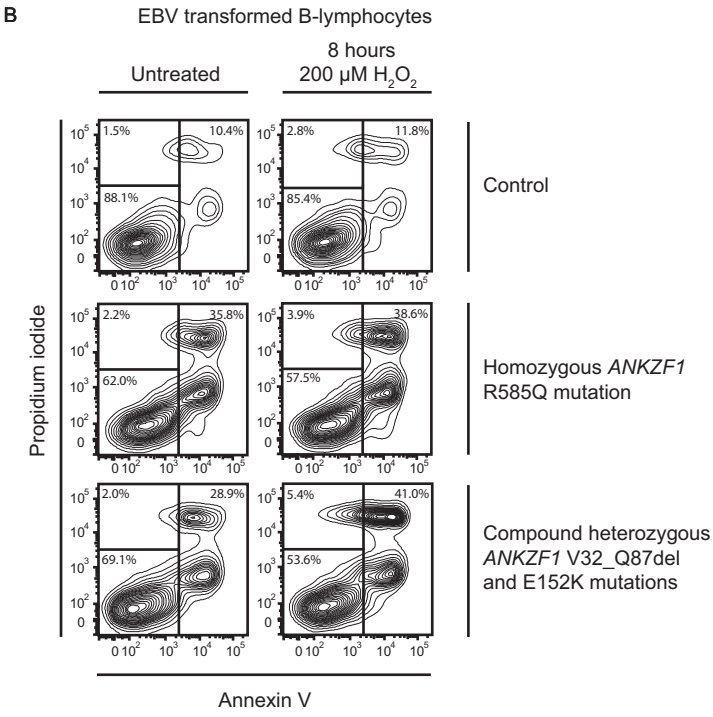
B
EBV transformed B-lymphocytes
Untreated
8 hours 200 μM H2O2
Propidium iodide
1.5% 10.4% 88.1%
2.8% 11.8% 85.4%
2.2% 35.8% 62.0%
3.9% 38.6% 57.5%
2.0% 28.9% 69.1%
5.4% 41.0% 53.6%
Control
Homozygous ANKZF1 R585Q mutation
Compound heterozygous ANKZF1 V32_Q87del and E152K mutations
Annexin V

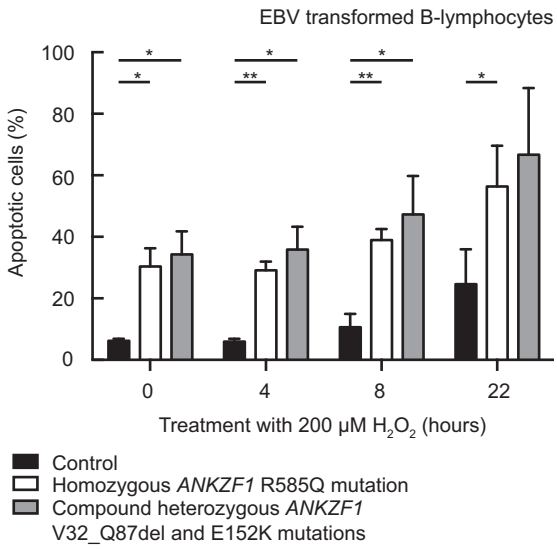
C
EBV transformed B-lymphocytes
Apoptotic cells (%)
100
80
60
40
20
0
0 4 8 22
Treatment with 200 μM H2O2 (hours)
Control
Homozygous ANKZF1 R585Q mutation
Compound heterozygous ANKZF1 V32_Q87del and E152K mutations

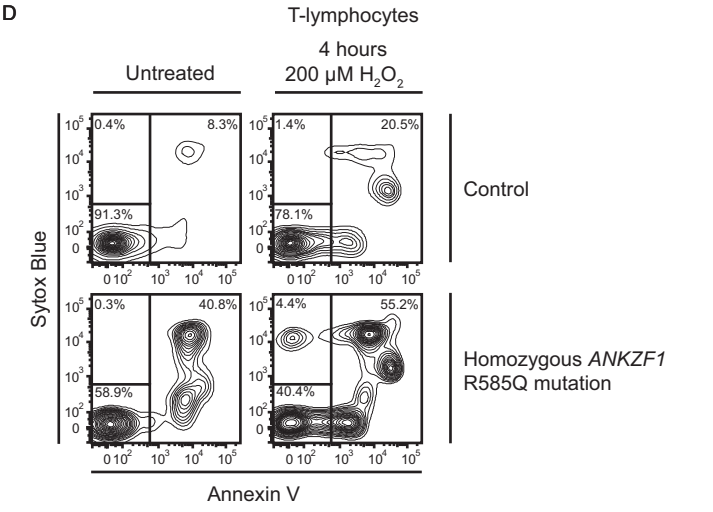
D
T-lymphocytes
Untreated
4 hours 200 μM H2O2
Sytox Blue
0.4% 8.3% 91.3%
1.4% 20.5% 78.1%
0.3% 40.8% 58.9%
4.4% 55.2% 40.4%
Control
Homozygous ANKZF1 R585Q mutation
Annexin V

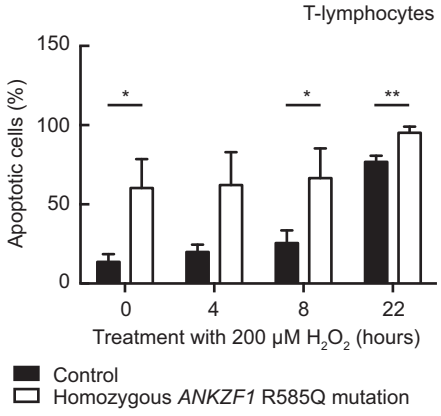
E
T-lymphocytes
Apoptotic cells (%)
150
100
50
0
0 4 8 22
Treatment with 200 μM H2O2 (hours)
Control
Homozygous ANKZF1 R585Q mutation

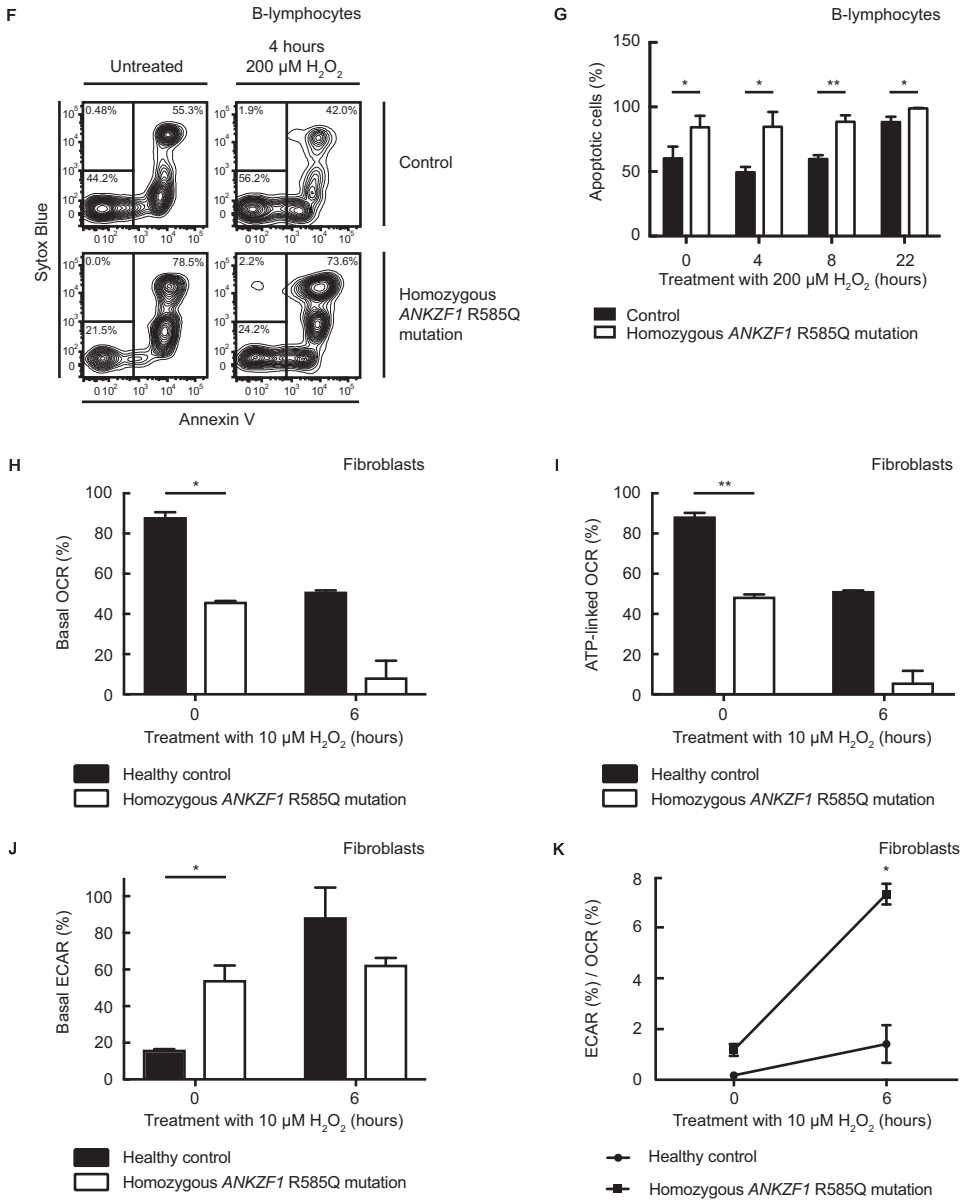

Figure 5—*continued*

growth. This inability of the Δ*Vms1* yeast strain to grow could be completely rescued by transformation of a construct containing Vms1 and partially but reproducibly rescued by transformation of a construct containing WT ANKZF1. However, ANKZF1 R585Q and ANKZF1 E152K were unable to rescue *Vms1* deletion (Fig. 6*C*). Taken together, these data show that whereas ANKZF1 WT is able to functionally rescue BY4742 Δ*Vms1* yeast, both ANKZF1 R585Q and E152K are not, confirming that ANKZF1 R585Q and E152K impair ANKZF1 function, probably leading to loss of mitochondrial integrity and apoptosis.

Discussion

In this study, we, for the first time, link mutations in *ANKZF1* to IO IBD and provide the first functional characterization of this gene in mammals. Using a combination of homozygosity mapping and whole-exome sequencing, we identified a

Figure 5. Increased apoptosis in lymphocytes harboring ANKZF1 mutations. *A*, amplification of $7.5 \cdot 10^5$ EBV-transformed B-lymphocytes from a healthy control, a patient with the homozygous *ANKZF1* R585Q mutation, and a patient with compound heterozygous *ANKZF1* V32_Q87del and E152K mutations was determined on the indicated days. *B* and *C*, EBV-transformed B-lymphocytes from two healthy controls, a patient with homozygous *ANKZF1* R585Q mutation, and a patient with compound heterozygous *ANKZF1* V32_Q87del and E152K mutations were left untreated or treated with 200 μM H_2O_2 for 4, 8, or 22 h. The percentage of apoptotic cells was determined by FACS after staining with Annexin V and propidium iodide. *D–G*, PBMCs isolated from healthy controls and a patient with homozygous *ANKZF1* R585Q mutation were left untreated or treated with 200 μM H_2O_2 for 4, 8, or 22 h. The percentage of apoptotic cells was determined by FACS using Annexin V and Sytox Blue. T-lymphocytes were identified using anti-CD3 antibodies (*D* and *E*). B-lymphocytes were identified using anti-CD19 antibodies (*F* and *G*). Results are representative of three independent experiments. Average and S.D. (*error bars*) are shown. *H–K*, fibroblasts from a healthy control and a patient with homozygous *ANKZF1* R585Q mutation were left untreated or exposed to 10 μM H_2O_2 for 6 h. OCR (*H*), ATP-linked OCR (*I*), ECAR (*J*), and the ratio of basal ECAR and basal OCR (*K*) were determined using the XF-24 extracellular flux analyzer. OCR and ECAR are shown as percentages of the highest rate. Average and S.D. of triplicates of one experiment are shown. Results are representative of three independent experiments. *, $p \leq 0.05$; **, $p \leq 0.01$.

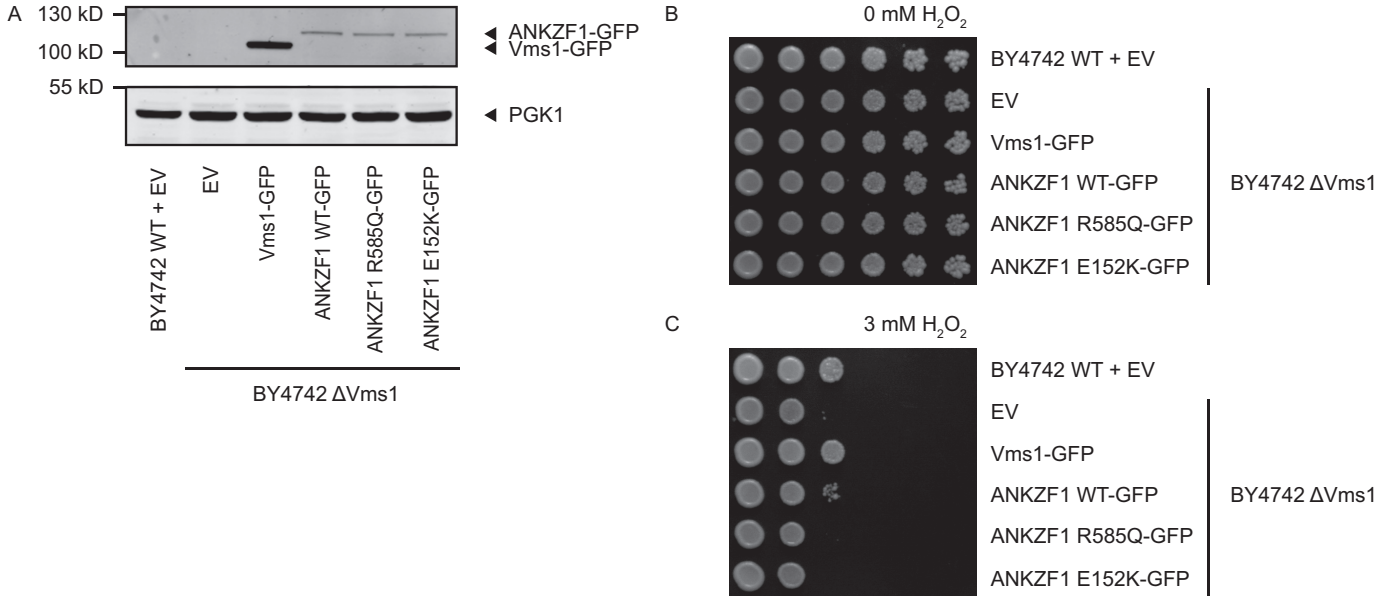

Figure 6. ANKZF1 R585Q and E152K are unable to functionally rescue Vms1-deficient yeast. *A*, protein expression of Vms1-GFP and ANKZF1-GFP in BY4742 WT and BY4742 ΔVms1 yeast strains transformed with indicated constructs determined by Western-blotting analysis using anti-GFP and anti-PGK1 antibodies. *B* and *C*, indicated yeast strains were grown overnight in SMD without uracil at 30 °C. Serial 5-fold dilutions of 0.4 A_{600} of each strain were grown on SMD plates without uracil and without H_2O_2 (*B*) or with 3 mM H_2O_2 (*C*) for 2 days at 30 °C. Results are representative of three independent experiments. *EV*, empty vector.

homozygous g.220100258G>A (*ANKZF1* p.R585Q) mutation in one IO IBD patient. In an additional IO IBD patient, we found compound heterozygous g.220096885G>A (*ANKZF1* p.V32_Q87del) and g.220097301G>A (*ANKZF1* p.E152K) mutations. Furthermore, two IO IBD patients carried a single heterozygous *ANKZF1* mutation: g.220094405C>T (located in the promotor) and g.220100539A>C (p.Q638P). Except for the g.220100258G>A mutation in the NHLBI, National Institutes of Health, ESP Exome Variant Server (EVS) and dbSNP databases, none of these mutations are described, and no frequency data are known. In the ExAC Browser Beta database for the g.220097301G>A mutation, an A allele frequency of $5{\cdot}10^{-5}$ is described. For the g.220100258G>A mutation in humans of European descent, the A allele frequency varies between 0.004 (dbSNP database, mutation added to NCBI dbSNP Build 135) and 0.01 (NHLBI ESP EVS and ExAC Browser Beta databases). This A allele frequency suggests that humans homozygous for the *ANKZF1* R585Q mutation can be free of symptoms, because no IBD patients with this mutation have been described before. Nevertheless, in our population of 13 IO IBD patients, four patients carried *ANKZF1* mutations on one or two alleles. When we only consider IBD with an onset before 6 months of age, the frequency of *ANKZF1* mutations in our study population is even 100%, suggesting that ANKZF1 is indeed important in the pathogenesis of IO IBD. We suggest that modifier genes may protect individuals with *ANKZF1* mutations against the development of IO IBD (20–22), explaining the low number of IO IBD patients with *ANKZF1* mutations found to date.

Although so far uncharacterized in mammalian cells, here we show that the function of ANKZF1 resembles the function of Vms1 in yeast. Vms1, the yeast homologue of ANKZF1, interacts with Cdc48, the yeast orthologue of VCP. In conditions of cellular stress, this complex is recruited to the mitochondrial membrane (16). We show that ANKZF1 also interacts with VCP and that this complex translocates to the mitochondria after exposure to H_2O_2 (Fig. 3, *A*–*D*). Here, Vms1 has a role in the degradation of mitochondrial proteins, and deficiency results in the accumulation of damaged and misfolded mitochondrial proteins, causing mitochondrial dysfunction and subsequently apoptosis (16). We propose that ANKZF1 has a similar function, because we found that ANKZF1 depletion leads to both a reduced mitochondrial integrity and mitochondrial respiration under conditions of cellular stress (Fig. 4, *B*–*G*). Furthermore, mammalian ANKZF1 was able to functionally replace yeast Vms1 in complementation assays, suggesting evolutionary conservation (Fig. 6*C*).

ANKZF1 mutations identified in both IO IBD patients with two mutated *ANKZF1* alleles cause impairment of ANKZF1 function, as shown by an increased level of apoptosis in patients' lymphocytes (Fig. 5, *B*–*G*), a decrease in mitochondrial respiration in patient fibroblasts with a homozygous *ANKZF1* R585Q mutation (Fig. 5, *H*–*K*), and an inability of ANKZF1 R585Q and E152K to rescue the phenotype of Vms1-deficient yeast (Fig. 6*C*). Dysfunction of ANKZF1 R585Q is the result of both reduced ANKZF1 mRNA and protein levels (Fig. 2, *A*–*C*) and a decreased translocation of ANKZF1 R585Q to the mitochondria in response to cellular stress (Fig. 3*B*). In contrast, in cells with compound heterozygous *ANKZF1* V32_Q87del and E152K mutations, ANKZF1 function is disturbed after recruitment of the VCP-ANKZF1 complex to the mitochondria, because mRNA and protein levels are unaffected in these cells (Fig. 2*D*) as well as interaction of ANKZF1 E152K with VCP and translocation of this complex to the mitochondria after induction of cellular stress (Fig. 3, *B*–*D*). Although it is unclear how the *ANKZF1* E152K mutation causes dysfunction, the *ANKZF1* V32_Q87del mutation occurs within an *in silico*-defined zinc finger, located near the N terminus of ANKZF1

(Fig. 1*F*). The exact function of this potential zinc finger has not been investigated yet, but it is highly conserved among several species. Normally associated with DNA binding, potentially disruption of the ANKZF1 zinc finger motif disrupts protein-protein interactions critical for ANKZF1 localization or function.

We demonstrate that loss-of-function mutations in *ANKZF1* are related to IO IBD, and dysfunction of ANKZF1 causes mitochondrial stress. Although mitochondrial stress has not previously been linked to the development of IO IBD, increased ER stress plays an important role in the pathogenesis of IBD (23–25). The unfolded protein response is a pathway activated by ER stress that facilitates the removal of unfolded and misfolded ER proteins (26). Dysfunction of the unfolded protein response leads to increased ER stress and the development of intestinal inflammation (23–25). Our data strongly suggest that besides ER stress, mitochondrial stress induced by loss of ANKZF1 function is also involved in the pathogenesis of IO IBD. However, further research is required to clarify the exact mechanism.

Although the pathway described in this paper has not previously been associated with IBD, mitochondrial pathology has been observed in IBD patients, including electron transport chain complex dysfunction (27–29), diminished mitochondrial-membrane potential (30), and changed mitochondrial morphology (31). Thus far, it has remained enigmatic whether these mitochondrial anomalies are a consequence of the disease or indeed contribute to pathology. However, in combination with the known link between mitochondrial stress and the development of a number of other immune diseases, this strongly suggests a role for mitochondrial stress in the pathogenesis of IBD. The genetic defect described in this paper for the first time provides a direct link between mitochondrial stress and the pathogenesis of IBD.

Taken together, we show that loss-of-function mutations in *ANKZF1* probably play a novel role in the pathogenesis of IO IBD. Furthermore, we characterize for the first time the function of ANKZF1 in mammals. These observations increase our understanding of the pathophysiology of IO IBD and underline the value of using modern sequencing techniques in this patient group. It also further highlights the potential role of mitochondrial stress in immunological disorders. Additional research is needed to further characterize the molecular pathway by which loss of ANKZF1 function causes intestinal inflammation.

Experimental procedures

Homozygosity mapping

Peripheral blood genomic DNA samples from the index patient and both parents were analyzed using Illumina HumanCytoSNP-12v2 arrays according to the manufacturer's protocol (Illumina Inc., San Diego, CA). Regions of homozygosity were determined using the BeadStudio® as well as our in-house analysis pipeline (scripts available upon request). Plug-in runs of at least 20 homozygous SNPs were compiled. Homozygous regions in the patient's genome were compared with regions from parents, and those exclusively found in the patient were retained and sorted according to size. Regions overlapping with centromeres were tagged. Regions spanning candidate genes for IBD (*CHUK*, *CYBA*, *CYBB*, *FERMT3*, *FOXP3*, *IKBKB*, *IKBKG*, *IL10*, *IL10RA*, *IL10RB*, *IL1A*, *IL1R1*, *IL2RA*, *IRAK4*, *ITGB2*, *LIG4*, *NCF1*, *NFKB1*, *NFKB2*, *NHEJ1*, *NOD2*, *RAG1*, *RAG2*, *RASGRP1*, *REL*, *RELA*, *RELAB*, *STAT3*, *STXBP2*, *TNFRSF13B*, and *WAS*) were examined for presence of a homozygous region in the patient.

Multiplexed whole-exome next-generation sequencing in a nuclear trio

Original genomic DNA was isolated from peripheral lymphocytes of the index patient and her parents. Genomic DNA concentration was determined using the Qubit Quant-iT™ method (Invitrogen), and 2000 ng of high-quality DNA of the trio was used for barcoded fragment library preparation and multiplexed enrichment for the SOLiD NGS platform using our in-house protocol (32). In brief, the DNA pool was fragmented using the Covaris™ S2 system (Applied Biosystems, Carlsbad, CA) to ~150-bp short fragments. After fragmentation, fragments were blunt-ended and phosphorylated at the 5′ end using the End-It™ DNA End-Repair Kit (EpiCenter, Madison, WI) and purified with the Agencourt AMPure XP system (Beckman Coulter Genomics, Danvers, MA) followed by ligation of double-stranded truncated versions of adaptors complementary to the SOLiD NGS platform. Ligation was performed using the Quick Ligation Kit (New England BioLabs, Ippswich, MA). After purification with the AMPure system, nick translation on non-phosphorylated and non-ligated 3′-ends, barcoding, and amplification in single PCR were performed for each library separately. The intensity of library bands was checked on 2% agarose gel (Lonza FlashGel System). PCR products were purified with the AMPure system to remove adaptor dimers and heterodimers. Amplified library fragments ranging from 175 to 225 bp were size-selected on 4% agarose gel, and gel slices were purified using the QIAquick Gel Extraction Kit (Qiagen, Hilden, Germany). Libraries of the trio were equimolarly pooled with two other barcoded libraries unrelated to this project ($n = 5$) and enriched in a multiplexed setup for the Agilent SureSelect Human All Exon 50Mb Kit (Agilent Technologies, Santa Clara, CA). Enriched library pool fragments were amplified using 12 PCR cycles and elongated to a full-length adaptor sequence required for SOLiD sequencing. All adaptor, primer, and barcode sequences are available in a previous publication (32). SOLiD sequencing was performed according to the SOLiD 4 manual to produce enough 50-bp reads to obtain sufficient coverage for a single allele in each library.

Variant detection and analysis

Raw sequencing reads were mapped against the human reference genome hg19/GRCh37 using our custom pipeline based on the Burrows-Wheeler Alignment algorithm. Single-nucleotide variants and small indels (≤7 nt) were called by our custom analysis pipeline as described before (33). The criteria for variant detection were set to enable also *de novo* heterozygous variants: minimal allele support based on 2 seeds of a read, strand balance set off, cut-off for coverage set to 10 reads, cut-off for non-reference allele (NRA) percentage set to 15%, and clonality filter that keeps maximally five clonal reads with the same start

site and removes reads above this level. All common and rare polymorphisms present in Ensembl62 (based on NCBI dbSNP Build 133 for humans) were tagged as known, and variants present in our in-house database (60 tested samples) were considered for sequencing errors or Dutch population-specific variants; other variants were considered to be novel and thus fulfill the criteria for ultra-rare disease. For each variant, location in genomic sequence, amino acid change, effect on the protein function, conservation score, and prediction programs (Polyphen, Polyphen2, SIFT, and Condel) were collected and subsequently used for prioritization for candidate variants. Three inheritance hypotheses were tested: 1) recessive with homozygous variant present in the affected child (NRA $>$ 75%) and heterozygous in parents (5% $<$ NRA $>$ 80%); 2) compound heterozygous, with one heterozygous allele inherited from the father and the second from the mother (5% $<$ NRA $>$ 80%); and 3) autosomal *de novo* with a heterozygous allele present only in the child (5% $<$ NRA $>$ 80%) and not inherited from the parents (NRA = 0). Confirmation of selected candidate mutations was performed by capillary sequencing, and primer information is available upon request.

Sanger sequencing

DNA of the index patient and 12 additional IO IBD patients was extracted from peripheral blood cells according to standard procedures. Testing of the coding sequences and exon-intron boundaries of the *ANKZF1* gene was performed by standard Sanger sequencing. Sequencing conditions and primer sequences are available upon request. Segregation analysis for the two patients with two mutated *ANKZF1* alleles was performed to confirm the expected inheritance pattern. Sanger sequencing of cloned cDNA synthesized from RNA isolated from peripheral blood of the patient with compound heterozygous *ANKZF1* V32_Q87del and E152K mutations was used to detect exon splicing consequences.

Antibodies and reagents

In this study, the following antibodies were used: rabbit anti-ANKZF1 (HPA035208, Sigma-Aldrich), mouse anti-tubulin (T9026, Sigma-Aldrich), mouse anti-TOM20 (612278, BD Biosciences), mouse anti-LC3 (0231-100, NanoTools, Teningen, Germany), mouse anti-p62 (sc-28359, Santa Cruz Biotechnology, Inc., Dallas, TX), goat anti-actin (sc-1616, Santa Cruz Biotechnology), goat anti-HA (A00168, GenScript, Piscataway, NJ), mouse anti-HA (H3663, Sigma-Aldrich), mouse anti-FLAG M2 (F3165, Sigma-Aldrich), rabbit anti-FLAG (F7425, Sigma-Aldrich), mouse anti-FLAG M2-peroxidase (HRP) (A8592, Sigma-Aldrich), mouse anti-GFP (11814460001, Roche, Basel, Switzerland), rabbit anti-phosphoglycerate kinase 1 (PGK1) (kindly provided by Dr. F. M. Reggiori), swine anti-rabbit immunoglobulins/HRP (P0399, Dako, Glostrup, Denmark), rabbit anti-mouse immunoglobulins/HRP (P0161, Dako), donkey anti-mouse IgG IRDye 680 (926-32222, LI-COR, Lincoln, NE), donkey anti-goat IgG IRDye 800CW (926-32214, LI-COR), donkey anti-rabbit IgG IRDye 680RD (926-68073, LI-COR), donkey anti-mouse IgG Cy5 (715-175-150, Jackson ImmunoResearch Laboratories, West Grove, PA), goat anti-rabbit IgG Alexa Fluor 568 (A11011, Invitrogen), goat anti-rabbit IgG Alexa Fluor 488 (A11008, Invitrogen), anti-human CD3-PE (555333, BD Pharmingen, San Diego, CA), anti-human CD14-PerCP/Cy5.5 (301824, BioLegend, San Diego, CA), and anti-human CD19-APC (555415, BD Pharmingen). 30% H_2O_2 was purchased from VWR (Radnor, PA), cycloheximide and hydroxychloroquine were from Sigma-Aldrich, and MG132 was from Cayman Chemical (Ann Arbor, MI).

Generation of plasmids

pcDNA3-FLAG-ANKZF1 was generated by adding restriction sites KpnI and XhoI and a FLAG tag to *ANKZF1* (HsCD00322220, Dana-Farber/Harvard Cancer Center, Boston, MA) and cloning a KpnI-XhoI fragment into the respective cloning site of pcDNA3 (Invitrogen). Using site-directed mutagenesis, the pcDNA3-FLAG-ANKZF1-R585Q and pcDNA3-FLAG-ANKZF1-E152K mutants were constructed. pcDNA3-HA-VCP was generated by adding restriction sites HindIII and NotI and an HA tag to *VCP* (HsCD00347285, Dana-Farber/Harvard Cancer Center) and cloning an HindIII-NotI fragment into the respective cloning site of pcDNA3. pMT2-FLAG-FOXP3 was described previously (34). pRS416-Vms1-GFP was generated by amplifying *Vms1* from genomic yeast DNA by PCR and adding restriction sites XhoI and BamHI to *Vms1*. *Vms1* was cloned into a pRS416 vector already containing a GFP tag at the C′ terminus (kindly provided by Dr. F. M. Reggiori). pRS416-ANKZF1-GFP was generated by adding restriction sites XhoI and BclI to *ANKZF1* and cloning it into the pRS416 vector already containing a GFP tag at the C′ terminus. In both pRS416-Vms1-GFP and pRS416-ANKZF1-GFP, the TPI promotor was cloned as a KpnI-XhoI fragment. Using site-directed mutagenesis, the pRS416-ANKZF1 R585Q-GFP and pRS416-ANKZF1 E152K-GFP mutants were constructed. pCAGGS-pOTC-GFP (kindly provided by Dr. R. C. Muise-Helmericks) has been described previously (35).

Cell culture

PBMCs were isolated from human peripheral blood by density gradient centrifugation using Ficoll-Paque Plus (GE Healthcare, Little Chalfont, UK) and cultured in Roswell Park Memorial Institute (RPMI) 1640 Medium with GlutaMAX (Life Technologies, Inc.) supplemented with 10% HyClone (Thermo Scientific, Waltham, MA), 100 units/ml penicillin (Gibco), 100 μg/ml streptomycin (Gibco), and 50 μM 2-mercaptoethanol (Sigma-Aldrich) at 37 °C and 5% CO_2.

B-lymphocytes were transformed with EBV to enable the performance of experiments with immortalized B-lymphocytes. To this end, PBMCs were cultured in RPMI 1640 Medium with GlutaMAX (Life Technologies) supplemented with 10% heat-inactivated FBS (GE Healthcare), 100 units/ml penicillin (Gibco), 100 μg/ml streptomycin (Gibco), and 50 μM 2-mercaptoethanol (Sigma-Aldrich) at 37 °C and 5% CO_2. Transduction was performed by adding 1 ml of supernatant containing EBV to 5–10·10^6 PBMCs in 1 ml of culturing medium. After 1 day, 10 μg/ml cyclosporin was added. When outgrowth of cells was observed, culturing medium was replaced. After 6 weeks, a fully transformed culture of B-lymphocytes was obtained.

Table 1
qRT-PCR primers

Gene	Forward primer	Reverse primer
ANKZF1	TCCTGTTCAGGCTCAGGGGAGAG	AGGGCAGACAGGAGAGGCTTGTC
β_2-Microglobulin	ATGAGTATGCCTGCCGTGTGA	GGCATCTTCAAACCTCCATG
GAPDH	AAATCCCATCACCATCTTCCA	CATGGTTCACACCCATGACGAA
HPRT1	TGACACTGGCAAAACAATGCA	GGTCCTTTTCACCAGCAAGCT
RPL13	CTATGACCAATAGGAAGAGCA	GCAGAGTATATGACCAGGTGG

U2OS cells (derived from human osteosarcoma cells) and HEK293FT cells (derived from human embryonal kidney cells) were cultured in DMEM with GlutaMAX and high glucose (Life Technologies) supplemented with 10% heat-inactivated FBS (GE Healthcare), 100 units/ml penicillin (Gibco), and 100 μg/ml streptomycin (Gibco) at 37 °C and 5% CO_2.

Fibroblasts were isolated from a skin biopsy according to a standard procedure used in the hospital. Thereafter, these cells were cultured as described for U2OS and HEK293FT cells.

shRNA viral transduction of U2OS cells

A lentiviral construct was used containing shRNA control (SHC002, Sigma-Aldrich) or shRNA targeting *ANKZF1* (TRCN0000150131, Sigma-Aldrich) and a puromycin resistance gene in the pLKO.1 vector. HEK293FT cells were grown in 10-cm dishes. After 1 day, lentivirus was produced by cotransfection of 5 μg of pLKO.1 vector containing shRNA, 1.8 μg of lentiviral packaging vector pLP/VSVG, and 3.25 μg of lentiviral packaging vector psPAX2 overnight using 50 μl of PEI (Polysciences Inc., Warrington, PA). The next day, the medium was replaced, and the cells were cultured for 24 h. The supernatant containing virus was collected and filtered through a 0.2-μm filter. Transduction was performed by adding 1 ml of viral supernatant, 1 ml of culturing medium, and 8 μg/ml Polybrene to $0.5{\cdot}10^5$ U2OS cells, which had been cultured overnight. After 1 day, the cells were washed with PBS, and new culturing medium was added. Selection was achieved by adding 1 μg/ml puromycin (Sigma-Aldrich).

Quantitative real-time polymerase chain reaction

RNA was isolated from different cell types using the RNeasy minikit (Qiagen) according to the manufacturer's protocol. cDNA was synthesized using the iScript cDNA synthesis kit (Bio-Rad) and amplified using SYBR Green supermix (Bio-Rad) in a MyIQ single-color real-time PCR detection system (Bio-Rad) according to the manufacturer's protocol. To quantify the data, the comparative *Ct* method was used. The relative quantity was defined as $2^{-\Delta\Delta Ct}$. β_2-Microglobulin, *GAPDH*, *HPRT1*, and *RPL13* were used as housekeeper genes. The average of the *Ct* values of these genes was used as reference. The primers are listed in Table 1.

Western blotting

Cells were lysed in Laemmli buffer (0.12 mol/liter Tris-HCl, pH 6.8, 4% SDS, 20% glycerol, 0.05 μg/μl bromphenol blue, 35 mmol/liter 2-mercaptoethanol) and incubated at 100 °C for 5 min. The protein concentration was measured by performing a Lowry protein assay. Equal amounts of proteins were separated by SDS-PAGE, transferred to a polyvinylidene difluoride membrane (Merck Millipore, Billerica, MA), blocked with 5% milk protein in TBST (0.3% Tween, 10 mM Tris, pH 8, and 150 mM NaCl in H_2O), and probed with primary antibodies as indicated in Table 2. The membranes were washed with TBST and incubated with appropriate secondary antibodies. Immunocomplexes were detected using enhanced chemoluminescence (GE Healthcare) or the LI-COR Odyssey imaging system.

Table 2
Antibodies for Western blotting

Antibody	Dilution
Goat anti-actin	1:5000
Rabbit anti-ANKZF1	1:1000
Mouse anti-FLAG	1:3000
Mouse anti-FLAG HRP	1:10,000
Mouse anti-GFP	1:3000
Goat anti-HA	1:2500
Mouse anti-LC3	1:1000
Mouse anti-p62	1:1000
Rabbit anti-PGK1	1:7500
Mouse anti-tubulin	1:10,000

Immunoprecipitation

U2OS cells were grown in 10-cm dishes for 1 day and transfected with a mixture of 1 μg of HA-VCP, 1 μg of FLAG-ANKZF1, and 10 μl of PEI overnight. The next day, the cells were washed with PBS and cultured for 24 h in medium. The cells were left untreated or treated with H_2O_2, washed twice with cold PBS, and lysed in radioimmune precipitation assay buffer (20 mM Tris, pH 7.4, 150 mM NaCl, 1% Nonidet P-40, 0.1% SDS, 5 mM EDTA) with 1% HALT protease inhibitor (Thermo Scientific). After a preclear using uncoupled protein G-agarose beads (Merck Millipore), 1:500 rabbit anti-FLAG antibody (Sigma-Aldrich) was added, and immunoprecipitation was performed using uncoupled protein G-agarose beads (Merck Millipore). The beads were washed three times in radioimmune precipitation assay buffer with 1% HALT protease inhibitor and sample buffer (0.12 mol/liter Tris-HCl, pH 6.8, 4% SDS, 20% glycerol, 0.05 μg/μl bromphenol blue, 35 mM 2-mercaptoethanol) was added. The samples were incubated at 100 °C for 5 min and subjected to Western blotting.

Confocal imaging

Localization studies—U2OS cells were seeded on poly-L-lysine (Sigma-Aldrich)-coated coverslips in a 6-well plate and untransfected or transfected with a mixture of 0.2 μg of FLAG-ANKZF1, 0.2 μg of HA-VCP, 0.2 μg of pOTC-GFP, and 3 μl of PEI per well. The cells were left untreated or treated with H_2O_2, washed with PBS, and fixed with 4% paraformaldehyde (VWR, Amsterdam, The Netherlands) for 30 min at room temperature. After quenching with 50 mM NH_4Cl (Merck) for 10 min, the cells were permeabilized in permeabilization buffer (PBS with 0.1% saponin (Sigma-Aldrich), 2% BSA (Sigma-Aldrich), 10% normal donkey serum (Jackson ImmunoResearch Labora-

Table 3
Antibodies for confocal imaging

Antibody	Dilution
Rabbit anti-ANKZF1	1:400
Rabbit anti-FLAG	1:500
Mouse anti-HA	1:500
Mouse anti-Tom20	1:750

tories), and, if cells were transfected, 10% normal goat serum (Jackson ImmunoResearch Laboratories)) for 10 min at room temperature. The cells were incubated with primary antibodies in permeabilization buffer for 60 min at room temperature as indicated in Table 3, after which they were washed three times with permeabilization buffer. The cells were incubated with appropriate secondary antibodies in permeabilization buffer for 60 min at room temperature, washed three times with permeabilization buffer, washed once with PBS and H_2O, and mounted in Prolong Gold with DAPI (Invitrogen). The samples were analyzed with a ×63 objective on a Zeiss LSM 700 fluorescence microscope.

Proximity ligation assay—PLA detection was performed according to the manufacturer's protocol (Olink Bioscience, Uppsala, Sweden). In short, U2OS cells grown on poly-L-lysine-coated coverslips in a 6-well plate were transfected with a mixture of 0.2 μg of FLAG-ANKZF1, 0.2 μg of HA-VCP, and 2 μl of PEI per well. The cells were left untreated or treated with H_2O_2, washed with PBS, fixed with 4% paraformaldehyde for 30 min at room temperature, quenched with 50 mM NH_4Cl for 10 min, and permeabilized in permeabilization buffer (PBS with 0.1% saponin, 2% BSA, and 10% normal donkey serum) for 10 min at room temperature. Cells were incubated with primary antibodies in permeabilization buffer for 60 min at room temperature as indicated in Table 3 and washed three times with permeabilization buffer. Cells were incubated with the secondary Duolink In Situ PLA Probe anti-mouse PLUS (Sigma-Aldrich) and Duolink In Situ PLA Probe anti-rabbit MINUS (Sigma-Aldrich) antibodies for 60 min at 37 °C in the dark and washed three times in a buffer containing 10 mM Tris, pH 7.5, 150 mM NaCl, and 0.05% Tween before detection of the probes using the Duolink In Situ PLA detection kit (Sigma-Aldrich). Cells were analyzed with a ×63 objective on a Zeiss LSM 700 fluorescence microscope.

Flow cytometry

Mitochondrial integrity—U2OS cells were seeded in a 24-well plate and left untreated or treated with H_2O_2. The cells were once washed with PBS, detached from the surface of the well using trypsin (Gibco), collected in a 96-well plate, and washed again with PBS. The cells were stained with 10 μg/ml rhodamine-123 (Invitrogen) in DMEM for 30 min at 37 °C, washed three times with PBS, and analyzed using the FACS Canto II cell analyzer (BD Biosciences).

Apoptosis—200,000 PBMCs or EBV-transformed B-lymphocytes were seeded in a 96-well plate. The cells were left untreated or treated with H_2O_2 and washed once with PBS. The cells were stained with 1:40 Annexin V FITC (Immunotools, Friesoythe, Germany) in 1× Annexin V binding buffer (BD Pharmingen) in the dark for 15 min at room temperature. PBMCs were also stained with 1:100 anti-human CD3-PE (BD Pharmingen) and 1:100 anti-human CD19-APC (BD Pharmingen) to distinguish different types of mononuclear cells. The cells were washed once with 1× Annexin V binding buffer, after which PBMCs were stained with 1:1000 Sytox Blue (Invitrogen) and EBV-transformed B-lymphocytes with 1:50 propidium iodide (Sigma-Aldrich). All samples were analyzed using the FACS Canto II analyzer (BD Biosciences).

Metabolic characterization

Per well of a poly-L-lysine-coated 24-well Seahorse culture plate, 50,000 U2OS cells or 160,000 fibroblasts were seeded. After 1 day, the cells were left untreated or treated with H_2O_2, and regular medium was replaced by XF medium, consisting of RPMI 1640 Medium (Life Technologies) supplemented with 10 mM glucose (Merck), 2 mM L-glutamine (Gibco), and 1 mM sodium pyruvate (Gibco). OCR and ECAR were measured at baseline and after treatment of the cells with 10 μM oligomycin (Seahorse Biosciences, North Billerica, MA), 1 μM carbonyl cyanide *p*-trifluoromethoxyphenylhydrazone (Seahorse Biosciences), and 100 μM rotenone (Seahorse Biosciences) using the XF-24 extracellular flux analyzer (Seahorse Biosciences).

Yeast assays

Yeast strains, growth media, and transformation—Saccharomyces cerevisiae strain BY4742 was used as WT strain. A BY4742 Δ*Vms1* yeast strain was commercially available. The yeast strains were grown in rich medium containing 1% yeast extract, 2% peptone, and 2% glucose. Empty vector pRS416 was transformed into the BY4742 yeast strain and empty vector pRS416, Vms1-GFP, ANKZF1-GFP WT, ANKZF1-GFP R585Q, or ANKZF1-GFP E152K in the BY4742 Δ*Vms1* yeast strain according to a standard procedure (36). The transformed yeast strains were grown in SMD (0.67% yeast nitrogen base, 2% glucose, and amino acids and vitamins as needed) lacking uracil.

Trichloroacetic acid (TCA) protein precipitation—Yeast strains were grown overnight in SMD lacking uracil at 30 °C. 2 A_{600} was collected and, after centrifugation, incubated with 500 μl of ice-cold 10% TCA for 30 min on ice. The yeast were spun, cold acetone was added to the pellet, and the pellet was resuspended by sonification. After incubation at 20 °C for 20 min, the yeast were spun and the pellet was dried. Glass beads, sample buffer, and 5 μl of 0.5 M ammonium acetate were added, and the samples were subjected to Western blotting.

Growth assay—Yeast strains were grown overnight in SMD lacking uracil at 30 °C. Serial 5-fold dilutions of 0.4 A_{600} were spotted on SMD plates lacking uracil without H_2O_2 or with 3 mM H_2O_2. The plates were incubated at 30 °C for 2 days.

Statistics

Statistical analysis was performed using the unpaired Student's *t* test with Welch's correction assuming a Gaussian distribution (Prism, GraphPad Software). A p value ≤ 0.05 was considered statistically significant.

Study approval

The study was approved by the institutional review boards of the University Medical Center Utrecht and the Hospital for

Sick Children (Toronto, Canada). All participants provided written informed consent for the collection of samples and subsequent analysis.

Author contributions—D. Y. v. H.-V., M. H., J. M. v. M., W. P. K., E. C., R. H. J. H., and P. J. C. designed the study. D. Y. v. H.-V., M. H., E. M., A. E., E. R., K. F., E. M. M. T., M. M. v. H., I. J. N., and W. P. K. performed the experiments. D. Y. v. H.-V., M. H., E. M., A. E., E. R., K. F., P. M. v. H., E. M. M. T., I. J. N., W. P. K., A. M. M., E. C., R. H. J. H., and P. J. C. analyzed the experiments. D. Y. v. H.-V., M. H., E. M., J. M. v. M., R. H. J. H., and P. J. C. wrote the manuscript. J. M. v. M., A. E., P. M. v. H., E. E. S. N., A. M. M., E. C., R. H. J. H., and P. J. C. critically revised the manuscript. Technical or material support was provided by J. M. v. M., M. M. v. H., A. M. M., and E. C.

Acknowledgments—We thank the members of the laboratory of Edwin Cuppen for technical support with genetic studies and the members of the laboratory of Paul Coffer for helpful discussions.

References

1. Kaser, A., Zeissig, S., and Blumberg, R. S. (2010) Inflammatory bowel disease. *Annu. Rev. Immunol.* **28,** 573–621
2. Khor, B., Gardet, A., and Xavier, R. J. (2011) Genetics and pathogenesis of inflammatory bowel disease. *Nature* **474,** 307–317
3. Xavier, R. J., and Podolsky, D. K. (2007) Unravelling the pathogenesis of inflammatory bowel disease. *Nature* **448,** 427–434
4. Levine, A., Griffiths, A., Markowitz, J., Wilson, D. C., Turner, D., Russell, R. K., Fell, J., Ruemmele, F. M., Walters, T., Sherlock, M., Dubinsky, M., and Hyams, J. S. (2011) Pediatric modification of the Montreal classification for inflammatory bowel disease: the Paris classification. *Inflamm. Bowel Dis.* **17,** 1314–1321
5. Heyman, M. B., Kirschner, B. S., Gold, B. D., Ferry, G., Baldassano, R., Cohen, S. A., Winter, H. S., Fain, P., King, C., Smith, T., and El-Serag, H. B. (2005) Children with early-onset inflammatory bowel disease (IBD): analysis of a pediatric IBD consortium registry. *J. Pediatr.* **146,** 35–40
6. Polito, J. M., 2nd, Childs, B., Mellits, E. D., Tokayer, A. Z., Harris, M. L., and Bayless, T. M. (1996) Crohn's disease: influence of age at diagnosis on site and clinical type of disease. *Gastroenterology* **111,** 580–586
7. Paul, T., Birnbaum, A., Pal, D. K., Pittman, N., Ceballos, C., LeLeiko, N. S., and Benkov, K. (2006) Distinct phenotype of early childhood inflammatory bowel disease. *J. Clin. Gastroenterol.* **40,** 583–586
8. Gilissen, C., Hoischen, A., Brunner, H. G., and Veltman, J. A. (2011) Unlocking Mendelian disease using exome sequencing. *Genome Biol.* **12,** 228
9. Ng, S. B., Nickerson, D. A., Bamshad, M. J., and Shendure, J. (2010) Massively parallel sequencing and rare disease. *Hum. Mol. Genet.* **19,** R119–R124
10. Ng, S. B., Buckingham, K. J., Lee, C., Bigham, A. W., Tabor, H. K., Dent, K. M., Huff, C. D., Shannon, P. T., Jabs, E. W., Nickerson, D. A., Shendure, J., and Bamshad, M. J. (2010) Exome sequencing identifies the cause of a mendelian disorder. *Nat. Genet.* **42,** 30–35
11. Glocker, E.-O., Kotlarz, D., Boztug, K., Gertz, E. M., Schäffer, A. A., Noyan, F., Perro, M., Diestelhorst, J., Allroth, A., Murugan, D., Hätscher, N., Pfeifer, D., Sykora, K.-W., Sauer, M., Kreipe, H., *et al.* (2009) Inflammatory bowel disease and mutations affecting the interleukin-10 receptor. *N. Engl. J. Med.* **361,** 2033–2045
12. Glocker, E.-O., Frede, N., Perro, M., Sebire, N., Elawad, M., Shah, N., and Grimbacher, B. (2010) Infant colitis: it's in the genes. *Lancet* **376,** 1272
13. Worthey, E. A., Mayer, A. N., Syverson, G. D., Helbling, D., Bonacci, B. B., Decker, B., Serpe, J. M., Dasu, T., Tschannen, M. R., Veith, R. L., Basehore, M. J., Broeckel, U., Tomita-Mitchell, A., Arca, M. J., Casper, J. T., *et al.* (2011) Making a definitive diagnosis: successful clinical application of whole exome sequencing in a child with intractable inflammatory bowel disease. *Genet. Med.* **13,** 255–262
14. Blaydon, D. C., Biancheri, P., Di, W.-L., Plagnol, V., Cabral, R. M., Brooke, M. A., van Heel, D. A., Ruschendorf, F., Toynbee, M., Walne, A., O'Toole, E. A., Martin, J. E., Lindley, K., Vulliamy, T., Abrams, D. J., *et al.* (2011) Inflammatory skin and bowel disease linked to ADAM17 deletion. *N. Engl. J. Med.* **365,** 1502–1508
15. Avitzur, Y., Guo, C., Mastropaolo, L. A., Bahrami, E., Chen, H., Zhao, Z., Elkadri, A., Dhillon, S., Murchie, R., Fattouh, R., Huynh, H., Walker, J. L., Wales, P. W., Cutz, E., Kakuta, Y., *et al.* (2014) Mutations in tetratricopeptide repeat domain 7A result in a severe form of very early onset inflammatory bowel disease. *Gastroenterology* **146,** 1028–1039
16. Heo, J.-M., Livnat-Levanon, N., Taylor, E. B., Jones, K. T., Dephoure, N., Ring, J., Xie, J., Brodsky, J. L., Madeo, F., Gygi, S. P., Ashrafi, K., Glickman, M. H., and Rutter, J. (2010) A stress-responsive system for mitochondrial protein degradation. *Mol. Cell* **40,** 465–480
17. van Loosdregt, J., Fleskens, V., Fu, J., Brenkman, A. B., Bekker, C. P. J., Pals, C. E. G. M., Meerding, J., Berkers, C. R., Barbi, J., Gröne, A., Sijts, A. J. A. M., Maurice, M. M., Kalkhoven, E., Prakken, B. J., Ovaa, H., *et al.* (2013) Stabilization of the transcription factor Foxp3 by the deubiquitinase USP7 increases Treg-cell-suppressive capacity. *Immunity* **39,** 259–271
18. Parsons, M. J., and Green, D. R. (2010) Mitochondria in cell death. *Essays Biochem.* **47,** 99–114
19. Youle, R. J., and van der Bliek, A. M. (2012) Mitochondrial fission, fusion, and stress. *Science* **337,** 1062–1065
20. Dipple, K. M., and McCabe, E. R. (2000) Phenotypes of patients with "simple" Mendelian disorders are complex traits: thresholds, modifiers, and systems dynamics. *Am. J. Hum. Genet.* **66,** 1729–1735
21. Nadeau, J. H. (2001) Modifier genes in mice and humans. *Nat. Rev. Genet.* **2,** 165–174
22. Romeo, G., and McKusick, V. A. (1994) Phenotypic diversity, allelic series and modifier genes. *Nat. Genet.* **7,** 451–453
23. Adolph, T.-E., Niederreiter, L., Blumberg, R. S., and Kaser, A. (2012) Endoplasmic reticulum stress and inflammation. *Dig. Dis.* **30,** 341–346
24. Kaser, A., Lee, A.-H., Franke, A., Glickman, J. N., Zeissig, S., Tilg, H., Nieuwenhuis, E. E. S., Higgins, D. E., Schreiber, S., Glimcher, L. H., and Blumberg, R. S. (2008) XBP1 links ER stress to intestinal inflammation and confers genetic risk for human inflammatory bowel disease. *Cell* **134,** 743–756
25. Kaser, A., Martínez-Naves, E., and Blumberg, R. S. (2010) Endoplasmic reticulum stress: implications for inflammatory bowel disease pathogenesis. *Curr. Opin. Gastroenterol.* **26,** 318–326
26. Ron, D., and Walter, P. (2007) Signal integration in the endoplasmic reticulum unfolded protein response. *Nat. Rev. Mol. Cell Biol.* **8,** 519–529
27. Restivo, N. L., Srivastava, M. D., Schafer, I. A., and Hoppel, C. L. (2004) Mitochondrial dysfunction in a patient with crohn disease: possible role in pathogenesis. *J. Pediatr. Gastroenterol. Nutr.* **38,** 534–538
28. Santhanam, S., Rajamanickam, S., Motamarry, A., Ramakrishna, B. S., Amirtharaj, J. G., Ramachandran, A., Pulimood, A., and Venkatraman, A. (2012) Mitochondrial electron transport chain complex dysfunction in the colonic mucosa in ulcerative colitis. *Inflamm. Bowel Dis.* **18,** 2158–2168
29. Sifroni, K. G., Damiani, C. R., Stoffel, C., Cardoso, M. R., Ferreira, G. K., Jeremias, I. C., Rezin, G. T., Scaini, G., Schuck, P. F., Dal-Pizzol, F., and Streck, E. L. (2010) Mitochondrial respiratory chain in the colonic mucosal of patients with ulcerative colitis. *Mol. Cell Biochem.* **342,** 111–115
30. Beltrán, B., Nos, P., Dasí, F., Iborra, M., Bastida, G., Martínez, M., O'Connor, J.-E., Sáez, G., Moret, I., and Ponce, J. (2010) Mitochondrial dysfunction, persistent oxidative damage, and catalase inhibition in immune cells of naïve and treated Crohn's disease. *Inflamm. Bowel Dis.* **16,** 76–86
31. Nazli, A., Yang, P.-C., Jury, J., Howe, K., Watson, J. L., Söderholm, J. D., Sherman, P. M., Perdue, M. H., and McKay, D. M. (2004) Epithelia under metabolic stress perceive commensal bacteria as a threat. *Am. J. Pathol.* **164,** 947–957
32. Harakalova, M., Mokry, M., Hrdlickova, B., Renkens, I., Duran, K., van Roekel, H., Lansu, N., van Roosmalen, M., de Bruijn, E., Nijman, I. J., Kloosterman, W. P., and Cuppen, E. (2011) Multiplexed array-based and in-solution genomic enrichment for flexible and cost-effective targeted next-generation sequencing. *Nat. Protoc.* **6,** 1870–1886

33. Nijman, I. J., Mokry, M., van Boxtel, R., Toonen, P., de Bruijn, E., and Cuppen, E. (2010) Mutation discovery by targeted genomic enrichment of multiplexed barcoded samples. *Nat. Methods* **7,** 913–915
34. van Loosdregt, J., Vercoulen, Y., Guichelaar, T., Gent, Y. Y. J., Beekman, J. M., van Beekum, O., Brenkman, A. B., Hijnen, D.-J., Mutis, T., Kalkhoven, E., Prakken, B. J., and Coffer, P. J. (2010) Regulation of Treg functionality by acetylation-mediated Foxp3 protein stabilization. *Blood* **115,** 965–974
35. Yano, M., Kanazawa, M., Terada, K., Namchai, C., Yamaizumi, M., Hanson, B., Hoogenraad, N., and Mori, M. (1997) Visualization of mitochondrial protein import in cultured mammalian cells with green fluorescent protein and effects of overexpression of the human import receptor Tom20. *J. Biol. Chem.* **272,** 8459 – 8465
36. Gietz, R. D., and Schiestl, R. H. (2007) High-efficiency yeast transformation using the LiAc/SS carrier DNA/PEG method. *Nat. Protoc.* **2,** 31–34